Optical Engineering

OpticalEngineering.SPIEDigitalLibrary.org

Survey of terahertz photonics and biophotonics

Kiarash Ahi
Nathan Jessurun
Mohammad-Parsa Hosseini
Navid Asadizanjani

SPIE.

Kiarash Ahi, Nathan Jessurun, Mohammad-Parsa Hosseini, Navid Asadizanjani, "Survey of terahertz photonics and biophotonics," *Opt. Eng.* **59**(6), 061629 (2020), doi: 10.1117/1.OE.59.6.061629

REVIEW

Survey of terahertz photonics and biophotonics

Kiarash Ahi,[a,*] Nathan Jessurun,[b] Mohammad-Parsa Hosseini,[c] and Navid Asadizanjani[b]

[a]University of Connecticut, Storrs, Connecticut, United States
[b]University of Florida, Department of Electrical and Computer Engineering, Gainesville, Florida, United States
[c]Santa Clara University, Santa Clara, California, United States

Abstract We review the advances of terahertz (THz) science and technology in biophotonics, including related challenges and solutions. The main impediment to THz spectroscopy and imaging in this field is the high absorption of the THz beam in water. Hence, transmission imaging and spectroscopy of thick wet tissue using THz radiation has generally been quite difficult. However, the absorption of THz waves by water molecules is so strong that increasing the power of the THz source can lead to structural and functional changes in tissues, so solutions must go beyond a larger power output. In terms of resolution, THz imaging is superior to ultrasound but inferior to visible light microscopy. Owing to its unique material analysis capabilities, promising diagnosis applications have been demonstrated through THz imaging and spectroscopy. Unfortunately, many applications are limited by beam penetration depth and resolution. Hence, researchers from a wide variety of scientific and technical fields have been actively improving these features through the development of electronic devices and materials. In addition, groundbreaking optical architecture and materials to reduce beam absorption in the optics of a system and generate focused beams with smaller diameters have been proposed. On the software side, image processing techniques to computationally enhance the resolution and quality of THz imaging have been proposed. Data science and machine learning to automate the diagnosis of defects and diseases through processing THz images and spectroscopy data have been proposed. We have reviewed the applications of THz radiation in biophotonics and research achievements toward advancing these applications. A conclusion with a roadmap toward increasing the footprint of the THz technology in biophotonics is also proposed. [DOI: 10.1117/1.OE.59.6.061629]

Keywords: terahertz; imaging; spectroscopy; characterization; plasmonic antenna; biophotonics.

Paper 191600SSV received Nov. 14, 2019; accepted for publication Apr. 9, 2020; published online May 22, 2020.

1 Introduction

The terahertz (THz) frequency range is located between radiofrequency and infrared—a largely unreachable bandwidth for many decades. Conventional electronics were incapable of generating such high frequencies, while photonic devices could not emit low enough frequencies. As such, no known wave generators could reach into this regime. Fortunately, research achievements in the late twentieth century finally broke through the THz frequency range.[1] Promising medical and industrial applications of THz technology soon followed. New systems such as THz time-domain spectroscopy (TDS) were developed as well. THz TDS is powerful for material spectroscopy, layer inspection, and transmission imaging of packaged objects.[2] THz-TDS systems are utilized in authentication,[3–5] nondestructive inspection,[6–17] three-dimensional (3-D) imaging,[18–20] quality control,[21–25] airport security,[26–32] art investigations,[33–36] detecting damages on wood caused by insects,[37] tomography,[38–43] characterization of astrophysical ice,[44] biomedical diagnosis and imaging,[45–53] assessment of burn injuries,[54,55] material characterization,[56–62] thickness measurements,[63,64] aerospace application,[65] detection of the dielectric function in biological fluids,[66] and holography.[67,68] Although the resolution of THz spectroscopy and imaging is

*Address all correspondence to Kiarash Ahi, E-mail: kiarash.ahi@uconn.edu

0091-3286/2020/$28.00

significantly higher than that of ultrasound and radiofrequency, its depth of penetration is limited as the absorption of the beam inside materials increases exponentially with respect to the frequency of the photons. Hence, increasing both the photon density and frequency of emission has been the primary focus of researchers in the device sector. In biophotonics applications, challenges for THz imaging and spectroscopy are even more significant as molecules of water have high absorption in the THz regime. The strong absorption of THz waves by water molecules means that significantly more photons must be emitted to maintain respectable signal-to-noise ratio (SNR) and depth penetration. However, increasing the power of the THz source can lead to structural and functional changes in tissues.[69] To tackle this challenge, THz measurements on wet tissues are primarily done in reflection mode. Alternatively, thin slices of tissues or dried tissues can be imaged in transmission mode. As compared with optical and x-ray imaging, the resolution of THz is limited due to the low frequency of the THz photons. Considering the frequency of visible light in the color red to be 428 THz and the upper limit of the commonly used THz beam to be around 4 THz, the resolution of THz images is at least 100 times lower than that of images captured in visible light. As mentioned earlier, THz imaging and spectroscopy have been demonstrated to offer promising applications for industrial and medical fields. To fit this ever-increasing range of applications, researchers from different fields have consistently worked toward improving the resolution and photon density of the beam in THz spectroscopy and imaging. In this respect, research groups in the photonics and electron device sectors have proposed several innovative device architectures and semiconductor materials. Researchers in the field of optics have developed innovative architectures of optical setups and lenses toward achieving high numerical aperture and low absorption. Groups in image processing and computer data processing have developed computational techniques for improving the resolution of the THz spectroscopy and imaging. Data scientists have developed automated software programs for analyzing THz measurements and improving the results. These efforts and achievements are reviewed in this paper.

This paper is organized as follows: in Sec. 2, the applications of THz in biological and biomedical fields and related challenges are discussed. In addition, research endeavors toward solving these challenges are reviewed. Section 3 outlines advances in devices and materials for generating THz radiation with higher frequencies and higher power. In Sec. 4, improvements in THz optics and image processing are reviewed. Section 5 concludes and summarizes the main ideas of this paper.

2 Terahertz Applications and Challenges in Biophotonics

2.1 *Defining Biophotonics and Exploring Current Imaging Techniques*

Biophotonics involves the study of optical processes in biological systems.[70] As such, this paper's focus is restricted largely to imaging biological samples, analysis of organic material transmission/reflectance characteristics, and similar applications.

The THz spectrum is not unique in its ability to perform subsurface biophotonic imagery. Multiple techniques such as x-ray, positron emission tomography (PET) scans, magnetic resonance imaging (MRI), and cytometry already fill this role. However, THz technology is the first to do so with remarkably low cost and danger relative to these methods. Moreover, some materials (notably water molecules) attenuate electromagnetic waves in the THz spectrum quite differently than at higher frequencies, giving THz imaging a unique window into spectral analysis that is difficult to achieve using alternative imaging methods. An example of this absorption profile is shown in Fig. 1, which shows the level of attenuation in water at various THz frequencies.

Although the degrading effect of intense THz radiation on DNA is reported,[72–75] no other detrimental effects are observed and THz is still safer than x-ray in many areas. These biomedical applications of THz technology were not possible at its inception in the 1960s. The initial generated frequencies were not coherent enough to draw significant conclusions from received data, and proper tools for processing the data were not yet in existence. However, the 1990s brought about significant improvements to TDS and femtosecond lasers, which drastically improved sensing capabilities at this frequency.[76] These new tools allowed researchers to send and receive individual wave pulses, providing spectral information in a broader frequency range and faster

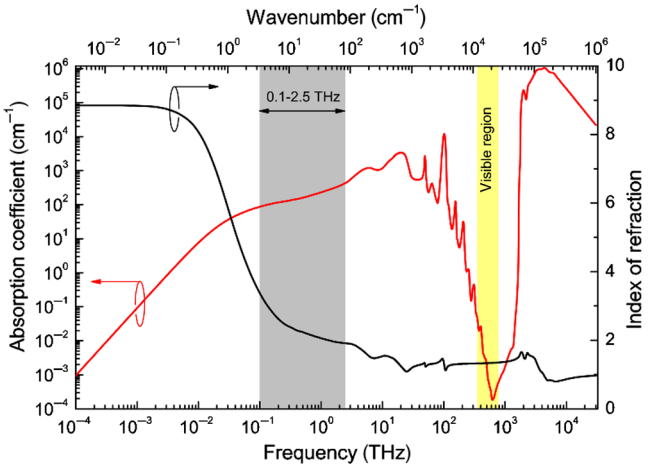

Fig. 1 Attenuation coefficients for water across various frequencies. Note that absorption in the THz band is uniquely higher than the surrounding regions. Bandwidths in this region offer unique insights into the characteristics of water-saturated materials. Figure retrieved from Ref. 71 with permission from OSA Publishing.

analysis than previous technology. Further developments such as nanoantenna arrays and plasmonic sensors continue this trend and allow increasingly complex biophotonic analysis. Several uses of THz technology are outlined below, including both past and current capabilities.

2.2 *Evaluating Crop Health*

As previously mentioned, water molecules dominate the absorption profile for THz waves. Early THz technology was adept at capturing this profile due to its propensity for high SNR values. In a scenario in which competing factors determine overall THz attenuation, the presence of water will dwarf most other impedance factors. Since healthy plants must contain an abundance of water in their cells to maintain rigidity, this should be clearly visible in a THz image of crops or individual plant samples. In 1995, Hu and Nuss[77] showed that visually indistinguishable leaf samples with substantially different levels of hydration can easily be classified using this method.[77–80] Figure 2 shows this effect in a leaf 48 h after it has been cut, in which it attenuates significantly less energy after dehydrating.[77] Notably, this image is indicative of contrast levels

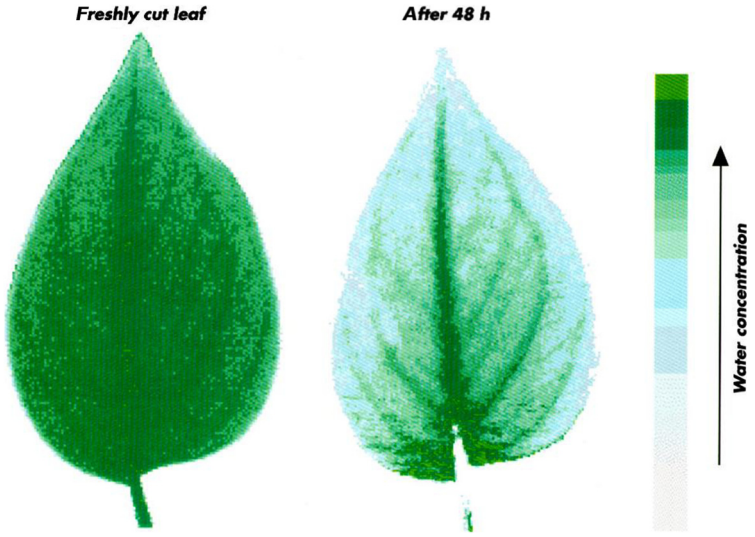

Fig. 2 THz images of a leaf after it is just cut and after 48 h. Lighter colors indicate less water is present. This figure demonstrates that, even at the dawn of THz imaging, it had tremendous potential for biological analysis. Retrieved from Ref. 77 with permission from *Optics Letters*.

attainable even in early prototypes of THz imaging technology. More recently, Born et al.[81] implemented a rigorous demonstration of the same effect in 2014. By correlating the relationship between THz transmission and plant stress in European conifers, they confirmed a strong relationship between sample thickness, harvest time, and transmission levels.[81] Water content is also an important characteristic in separating genetically modified organism crop strains from their nonmodified counterparts. In 2016, Liu et al.[82] found that THz transmission profiles were crucial in nondestructive detection of transgenic rice seeds. On a larger scale, THz spectroscopy offers a useful window into determining crop hydration—a major indicator of overall vitality.[83–86] In one study, Castro-Camus et al.[87] assessed the feasibility of several irrigation techniques across a variety of plant species. In contrast to alternative measurement techniques, TDS allowed them to measure several aspects of individual and group plant health without altering the samples in the process.[87]

2.3 *Early Indicators of Abnormal Tissue*

After the developments in THz technology in the late 1990s, applications in this bandwidth became far more feasible. Owing to the extremely important factor that water plays in biological material, THz imagery offers key insights into organic processes that cannot be viewed easily using alternative methods. By the mid-2000s, researchers improved imaging techniques to view quantitative measures of sample water content, not just its presence or absence. As a result, they could make helpful insights into the characteristics of these samples, such as the two examples shown below.

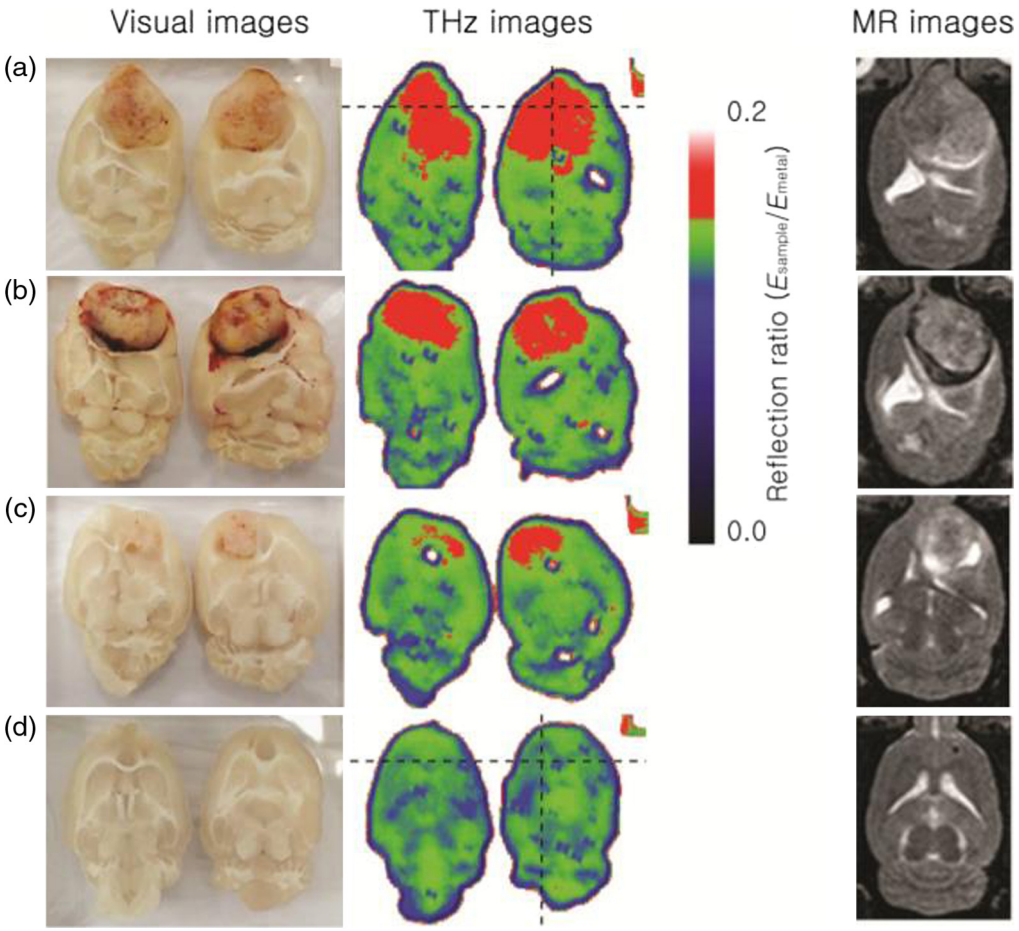

Fig. 3 THz and MRI images of brains (a)–(c) with and (d) without tumors. Note that THz imaging is highly adept at locating both presence and size of tumors. Image retrieved from Ref. 88 with permission from the Optical Society of America.

2.3.1 *Cancerous growths*

At the beginning stages of many tumors, it is difficult to visually distinguish healthy tissues from benign or malignant growths. However, cancerous cells typically house more water than their healthy counterparts. As a result, THz imaging can provide contrast that is nearly impossible to achieve with other imaging modalities. In 2014, Oh et al.[88] demonstrated this capability in an analysis of brain tumors. Comparing THz images with traditional MRI scanning methods, they make evident the clearly superior contrast inherent in THz profiles. These findings are depicted in Fig. 3, which shows that THz capabilities are more effective than MRI scans for quantitatively analyzing brain tumors. It is worth stressing that these pictured samples did not have to be stained or specially prepared prior to THz imaging—they were obtained in a wholly nondestructive manner.[88]

This is a remarkable step forward in potentially providing preventative cancer screenings since THz imaging can be performed quickly and at a low cost.[79,89–96] *In-vivo* (samples on living organisms) measurements, though only effective for up to a few microns, are still effective enough to detect epidermal defects. In one instance, Zaytsev et al. successfully used this technique to noninvasively scan participants for the presence of melanoma in skin samples.[97] More forms of *in-vivo* analysis are provided in later sections.

2.3.2 *Osteoporosis*

Developments in THz sensing have also led to higher SNR during attenuation profile analysis. Kim et al.[89] leveraged this concept in 2011 to characterize healthy versus ossified bone tissue in the same sample. Figure 4 depicts these findings, in which THz scanning clearly denotes the unhealthy areas. As a healthy animal ages, its old bone tissue is replaced at a specific rate over time. Osteoporosis is a condition in which the body removes older bone tissue faster than it is

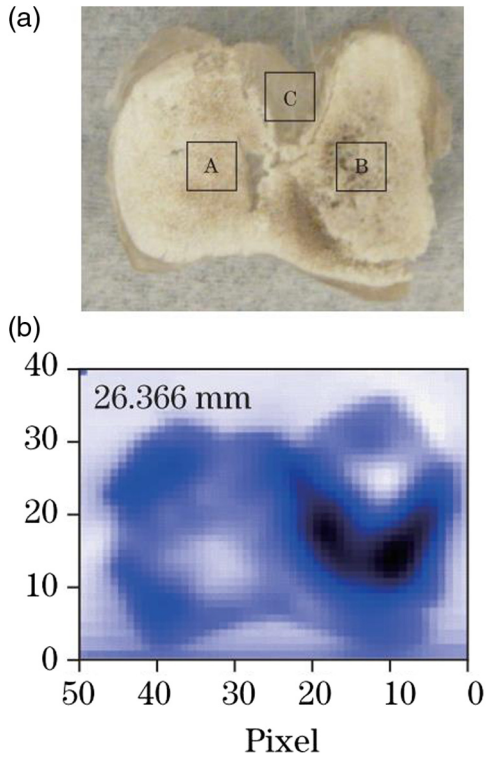

Fig. 4 Chicken bone sample. (a) Region A is normal spongy bone, region B is ossified, and region C contains cartilage. (b) The separate regions are clearly distinguishable in the THz reconstruction. Combination of two figures retrieved from Ref. 89 with permission from the OSA.

replaced, making the bone structure more brittle and porous over time. Unfortunately, the onset of this disease is often too gradual to detect reliably using conventional imaging approaches. As such, physicians rely on a combination of several metrics to evaluate the likelihood that an individual will be diagnosed with osteoporosis.[98] However, porous bone has a noticeably different attenuation signature in the THz bandwidth compared with healthy bone in the same specimen.[89,99–102] With further developments in THz sensing, *in-vivo* measurements may provide early, quantitative indicators of bone decay and improve patient care as the disease progresses.

2.4 *Measurements on Live Samples*

In the early stages of THz biophotonic applications, THz profiling was almost exclusively performed on excised and carefully prepared samples. However, recent advances have allowed high enough SNR for imaging live bodies. Importantly, these scans can be performed with minimal harm since THz radiation is nonionizing. Most applications in this regard involve identifying water concentration levels in various tissue samples to ascertain more information about the subject. To date, such specimens include rabbit corneal tissue,[91,92,103] rabbit and rat abdominal tissue (an example is shown in Fig. 5),[104,105] and human skin.[46,94,106–108] In all cases, exposure to THz radiation for the duration of the study yielded negligible harmful side effects. Berry et al. performed an in-depth study to ensure the safety of these scans, confirming minimal consequences.[109] Strides in this area also have promising applications in monitoring blood glucose levels for diabetic patients. From 2016 to 2019, multiple research groups have shown that THz spectroscopy scans remove the need for constant blood samples. Moreover, this method provides constant glucose level monitoring without the need for an intravenous system—increasing both safety and comfort for the subject.[46,108,110–115]

2.5 *Organic Chemical Bond Analysis*

As mentioned in the introduction to this section, many techniques used for imaging organic processes require the object to be identified and stained prior to the imaging procedure. This step is particularly inconvenient when working with very small-scale samples, such as DNA.[116] Fortunately, some organic bonds (such as the double-helix structure of DNA) have resonance patterns lying in the THz frequency region. As such, certain photonic excitations of these molecules allow THz waves to radiate from the sample for analysis in much the same way as the reflected wave from THz illumination. Similar procedures can be carried out on RNA, some proteins, and other polypeptide bonds.[79,117–119] Moreover, these measurements can be performed orders of magnitude faster than previous data collection techniques.[120]

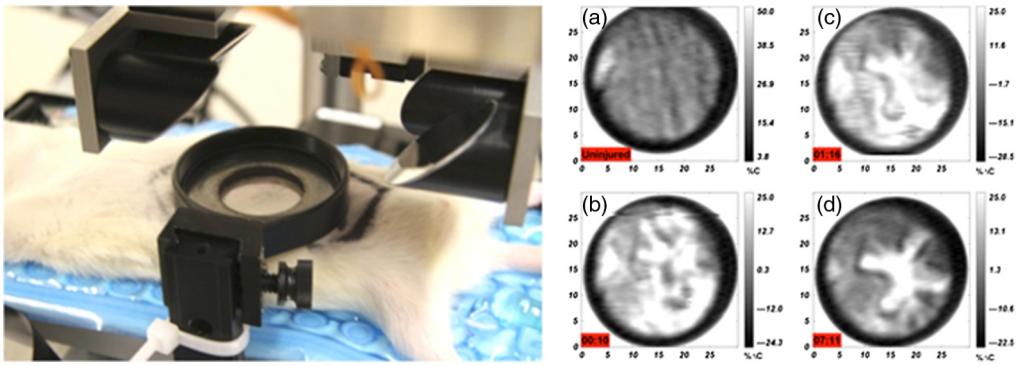

Fig. 5 Left: *In-vivo* setup for imaging a rat abdomen. The imaged area was branded and imaged at multiple timestamps. Right: THz images at (a) start, (b) 10 min, (c) 1 h, and (d) 7 h after branding the specimen. THz analysis provides sufficient information to reliably quantify the seriousness of such an injury. Figures retrieved from Ref. 105 with permission from SPIE.

2.5.1 *DNA/RNA*

The idea of using THz to analyze DNA structure has existed since the early 1990s.[121,122] Advantages to this technique include the lack of required staining and low-energy photons that do not require ionizing of molecules. As such, researchers could image cells for a longer period with fewer adverse effects compared with conventional techniques.[75,116,123,124] While it may not possess the resolution capabilities of the alternative methods, THz analysis is certainly sufficient for multiple forms of DNA characterization.[79,118,119,125,126] In contrast, one of the most effective alternative methods for analyzing DNA's helical bond involved fluorescence microscopy, a technique that stains subject molecules to give them enough contrast for viewing under an optical microscope. However, this damages the cells being imaged; as such, the sample cannot be used for long-term study.[127] X-ray imaging can also be used to study these samples but incurs damaging penalties as well due to its ionizing radiation, and it still requires the samples to be stained beforehand. Hence, further developments in THz spectroscopy are ideal for long-term studies of a single cell's nucleic acid.

2.5.2 *Protein interactions and amino acids*

THz-bandwidth vibrational modes are also quite informative at describing protein interactions. Previously, one of the best means of analyzing protein–molecule membrane interactions involved surface-phonon resonance and sample labeling.[128] However, it required rather large interacting molecules and a lengthy sampling duration to achieve analytical results. THz imaging decreases both requirements, allowing researchers to see interactions at even smaller molecule sizes with rapid sampling durations.[129–137] One such example is depicted in Fig. 6, where THz imaging achieved the same accuracy as fluorine labeling for detecting the presence of streptavidin protein bonding.

Once again utilizing the spectral analysis features of THz imaging, amino acids can be characterized in new and insightful manners through their transmission/reflectance profiles over a range of frequencies. This has led to more accurate descriptions of amino acid and polypeptide lattice structures and further verification of theoretical results.[96,108,129,138–141]

2.6 *Developments in Optical Coherence Tomography*

THz optical coherence tomography (OCT) leverages a combination of Michaelson interferometry with low-coherence THz beams to infer sample depth information. The basic setup behind this principle is illustrated in Fig. 7. During OCT imaging, photons from the source pass through a beam splitter to both the sample and a reference mirror. Information from both of these paths

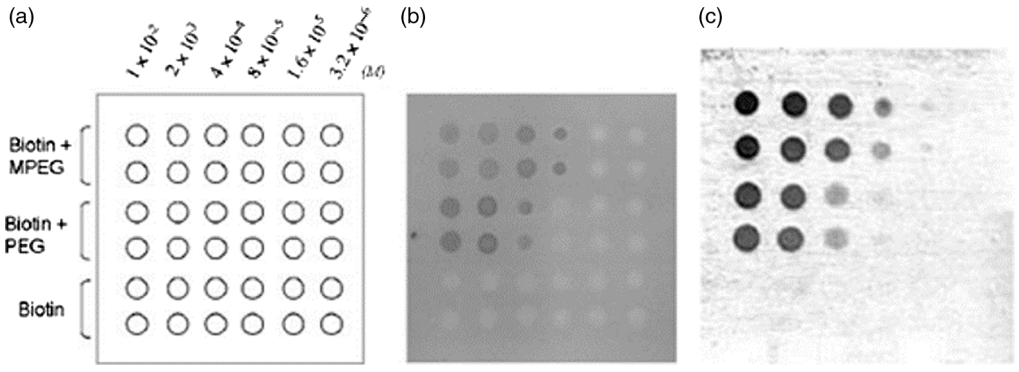

Fig. 6 Experiment showing THz profiling is as accurate as fluorine labeling in detecting protein bonding. (a) Grid layout of protein samples on a membrane slide. (b) Fluorine-labeled image. Dark spots indicate that a form of protein bonding to the membrane has occurred. (c) THz image of the same slide. As in (b), dark spots indicate the occurrence of bonding. Importantly, (c) can be obtained without staining the samples. Retrieved from Ref. 128 with permission from OSA Publishing.

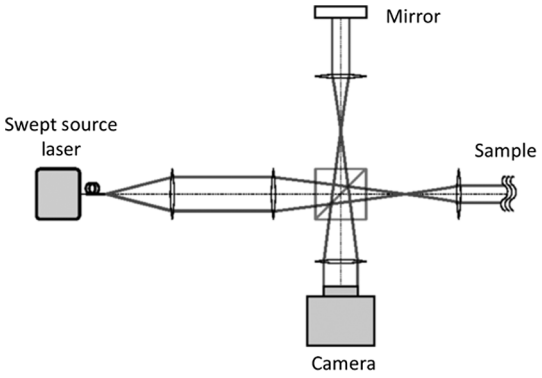

Fig. 7 Basic setup for interferometric imaging. THz OCT uses beams in the THz wavelength. A source beam passes through a splitter, which sends half of the energy to the sample and half to a mirror (reflective element). Retransmission from both the sample and mirror is picked up at the camera, where an interference pattern emerges. Retrieved from Ref. 143 with permission from OSA Publishing.

are combined in the processing stage, where constructive and destructive interferences yield valuable information about the sample's depth and composition characteristics.[142]

OCT is well suited for biological applications since its emission source is nonionizing. As such, it is safe to use for even extended durations on biological material. In effect, this imaging technique allows for the subsurface, volumetric capabilities of x-ray wavelengths without the same biological consequences.

Though OCT is available in a wide variety of smaller wavelengths, THz OCT in particular is well suited for biophotonic analysis. Unlike traditional shorter-wavelength OCT, THz wavelengths are less prone to scattering and allow significantly higher sample depth penetration.[144] It is also quite versatile, allowing for use in both time-domain (TD) and Fourier-domain (FD) imaging modes.

During TD OCT, the beamsplitting mirror must be mechanically moved over time. This movement causes changes in the interference pattern that coincide with different sample depths. In this manner, measurements at multiple sample depths can be performed.[145] In FD OCT (also known as swept-source OCT), the source sweeps through several THz wavelengths as the system characterizes the changes in interferometry. This newer development in THz OCT requires a smaller apparatus, offers higher resolution, and decreases acquisition time.[146]

Multiple independent THz sources can produce necessary power and spectral bandwidths for OCT imaging. Lee et al. proved that quantum cascade lasers (QCLs) were capable of this achievement in 2011, while Isogawa et al. showed in 2012 that uni-traveling-carrier photodiode modules were also successful sources.[147,148] In both cases, submillimeter depth resolution was provided on samples that scale well to biological analogs. Importantly, in each case, researchers corroborated OCT results with standard two-dimensional (2-D) THz imaging, ensuring that the results were accurate within an expected margin.

Implementations by Nagatsuma et al. proved sufficient for gathering depth information largely independent of the imaged medium. Especially relevant to biophotonic imaging, they successfully collected information about specimen water levels in their experimental setup.[149]

Recent publications such as Fitzgerald et al.'s study showed that THz OCT results can be combined with traditional THz-TDS measurements to infer unique sample properties. Moreover, this same method generated thickness estimates in two different forms, allowing confirmation checks for each measurement, as depicted in Fig. 8.[150]

In addition, efforts by Kitahara et al. showed that FD THz OCT complements traditional TD OCT. Signal processing advances in the field allowed them to provide reliable tomographic measurements despite substantial noise levels in their broadband THz source.[151]

In conclusion, the appropriate groundwork has been laid for efficient, robust, high-resolution THz OCT. Existing *in-vivo* applications for THz OCT allow for the imaging of skin and other external regions.[152] However, the ~10- to 150-μm-depth limitation currently prohibits its use in larger or deeper biomedical samples.

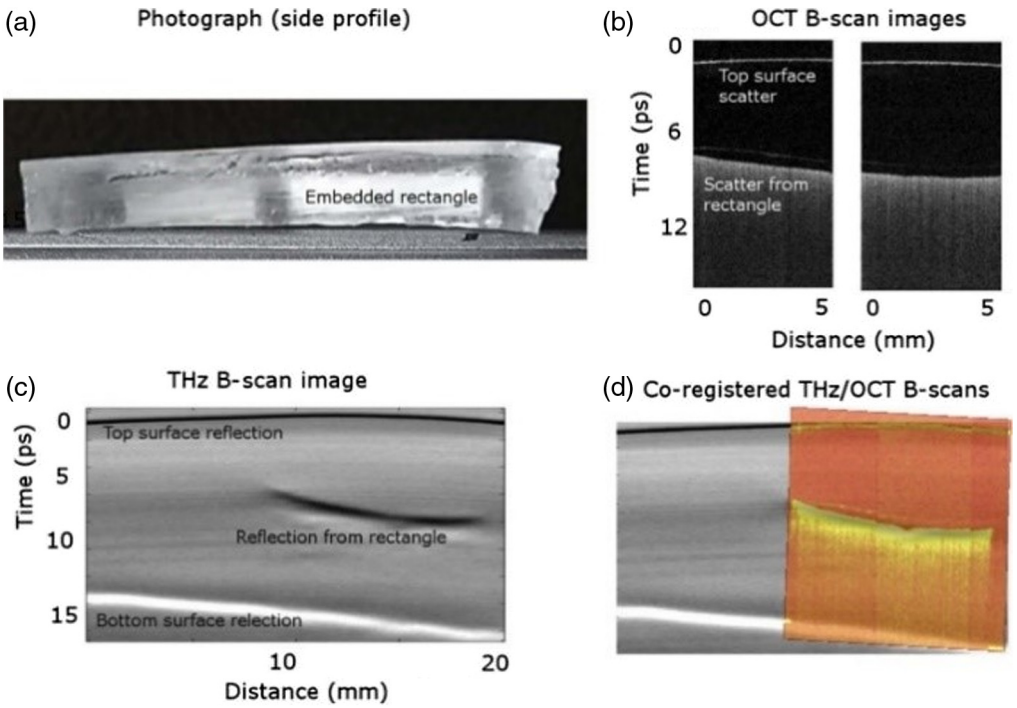

Fig. 8 The overlay of an OCT-acquired image on top of a THz scan visually confirms the similarity between these methods. Retrieved from Ref. 150 with permission from OSA.

3 Advances in Terahertz Devices and Materials

3.1 *Advances in Terms of Terahertz Devices*

In 1976, the first published THz image was generated using a THz gas laser with an emission frequency of 300 GHz.[153] Common methods of 1 to 5 THz bandwidth radiation involved rectifying the oscillations of the femtosecond lasers using a nonlinear crystal. In such a way, a pulse wave with a central frequency in the optical band and spectral width in the THz range can be downconverted into a pulse of THz radiation.[154] As mentioned in Sec. 1, the resolution of THz imaging is limited due to the low frequency of THz radiation as compared with the frequency of photons in visible light and x-ray. As the frequency of the radiation in the THz range increases, the absorption of photons in the material increases exponentially. In brief, for increasing the probability of detecting a higher number of high-frequency THz photons by a THz detector, the number of emitted high-frequency THz photons from the THz emitter, the sensitivity, and the frequency band of the detector need to increase. Hence, the main focus of research has been developing THz emitting devices capable of emitting THz radiation with higher photon densities and at the same time capable of emitting THz photons in higher frequency bands, together with developing THz sensors with higher detection frequency and higher sensitivities.

As mentioned, the THz beam has been traditionally generated through extracting the envelope of the oscillations in the femtosecond laser beam using a nonlinear crystal.[155] As nanotechnology advances, the tendency has been shifting toward photoconductive THz emitters and detectors.[156] In 1995, Hu and Nuss reported the first transmission of a THz image developed through optoelectronic THz TDS using photoconductive antennas.[77] As shown in Fig. 9, the function of photoconductive antennas in generating THz radiation is similar to that of nonlinear crystals.[156]

As shown in Fig. 10, photoconductive antennas of the emitter and detectors are made of metal electrodes fabricated on a photon-absorbing semiconductor substrate created for operating in the THz frequency range.[157,158] First, a femtosecond laser pulse pumps the emitter side photoconductive antenna. A bias voltage is applied to this antenna to drift the photogenerated carriers in the substrate active channel. As a result of this drift, an ultrafast photocurrent is induced between the two metallic arms of the antenna. The full width at half maximum (FWHM) of this

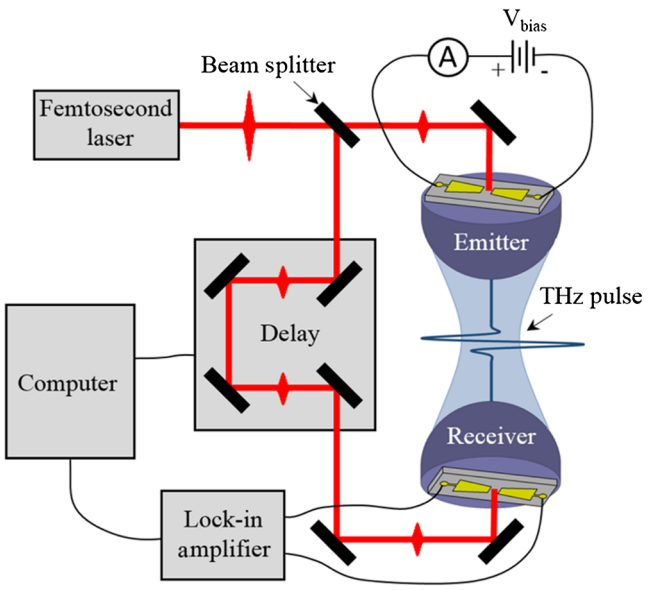

Fig. 9 Diagram of a THz TDS system, including photoconductive antennas, optical delay line, femtosecond laser, locked-in amplifier, and the computer. Reproduced with permission.[156] Copyright 2018, SPIE.

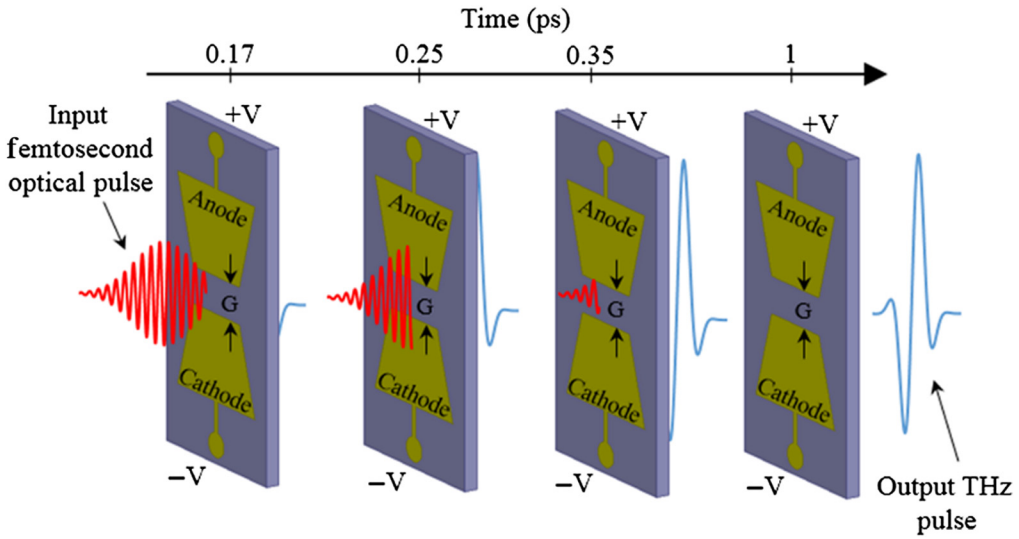

Fig. 10 Operation principle of photoconductive THz antenna. Reproduced with permission.[156] Copyright 2018, SPIE.

photocurrent is in the subpicosecond range. This photocurrent contains a frequency bandwidth in the THz range. This photocurrent drives the antenna, and as a result one pulse of electromagnetic radiation with the duration of subpicosecond, or the equivalent frequency range of a few THz, is emitted. As shown in Fig. 9, a beam splitter and an optical delay line are utilized to pump the detector antenna upon arrival of the THz pulse. When the active region absorbs a THz electromagnetic pulse, an electric field is induced. This electric field drifts the carriers between the electrodes of the antenna. In other words, a photocurrent pulse with a frequency range in the THz region is generated. As illustrated in Fig. 9, a lock-in amplifier, which is usually a proportional–integral–derivative controller, ensures that the rate of sensing repetition or frequency of sensing is locked on the repetition rate of the THz pulse and a computer is used for recording and displaying the pulse.[156] For operation in continuous-wave (CW) mode, a heterodyned dual-frequency optical beam with a frequency difference in the range of THz is used.[157]

To enhance the intensity of the emitted THz signal, the amount of the photogenerated carriers needs to increase. Similarly, to enhance the sensitivity of the THz detectors, the amount of the photogenerated carriers in the detector antenna needs to increase. To enhance the quantum efficiency of the THz photoconductive antenna, and hence the photon density of the THz beam, innovative architectures to improve the design of the photoconductive antennas were proposed and fabricated.[157,159] In the following sections, some of these devices are reviewed.

3.1.1 *Novel terahertz photoconductive antennas with higher photon efficiency*

In 2012, Park et al.[160] demonstrated that implanting nanorods into the active channel of a photoconductive antenna contributes to the increased concentration of the pumping femtosecond laser illumination inside the active region. The higher the number of the pumping photons reflected on the active region is, the higher the number of absorbed photons is, resulting in a larger amount of photocarrier generation and finally a larger number of emitted THz photons. In a similar procedure, the mentioned nanorods contribute to reflecting on the active region more photons of the received THz beam at the THz detector and contribute to enhancing the sensitivity of the detecting THz photoconductive antenna.[161–164] Figure 11 illustrates the structure and scanning electron microscopy (SEM) images of photoconductive THz antennas based on nanorods.[160]

In another effort for improving the design of the THz photoconductive antennas, contact electrodes were proposed to decrease the path between the two electrodes of the photoconductive antenna.[166,167] In this way, the carriers pass through a shorter distance in the active region of the substrate between the two electrodes. Hence, the transit distance and the time of the carriers in the active region is shorter and, as a result, the percentage of the carriers that successfully pass through the active region without going through recombination is increased. Consequently, the number of emitted THz photons is higher. In summary, adding plasmonic contact electrodes to the photoconductive THz antennas leads to THz devices with higher resolution and depth of penetration.[168–170] Such a design was first proposed by Berry and Jarrahi[167] in 2010. As illustrated in Fig. 12, the advanced structure of this plasmonic THz device contains large area photoconductive nanoantenna arrays. Since larger areas are available to be pumped by the femtosecond lasers, higher power and beam spot can be used without harmful carriers screening or thermal effects.[170–173] A radiation power of 3.8 mW over the 0.1- to 5-THz range of frequency

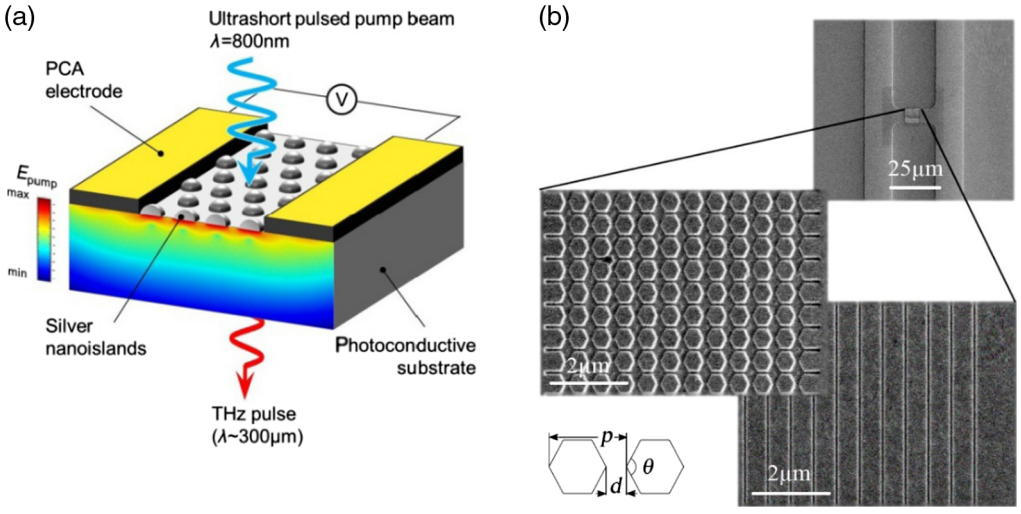

Fig. 11 (a) Photoconductive THz antennas with nanorods as light concentrators. Figure retrieved from Ref. 160 with permission from OSA Publishing. (b) SEM image of fabricated device, including the 20-μm dipole on SI-GaAs substrate (top SEM image), the active area of the hexagonal plasmonic array (middle SEM image), and the active area of the strip plasmonic array (lower SEM image). The diagram shows apex angle θ, gap size d, and periodicity p. Retrieved from Ref. 165 with permission from OSA Publishing.

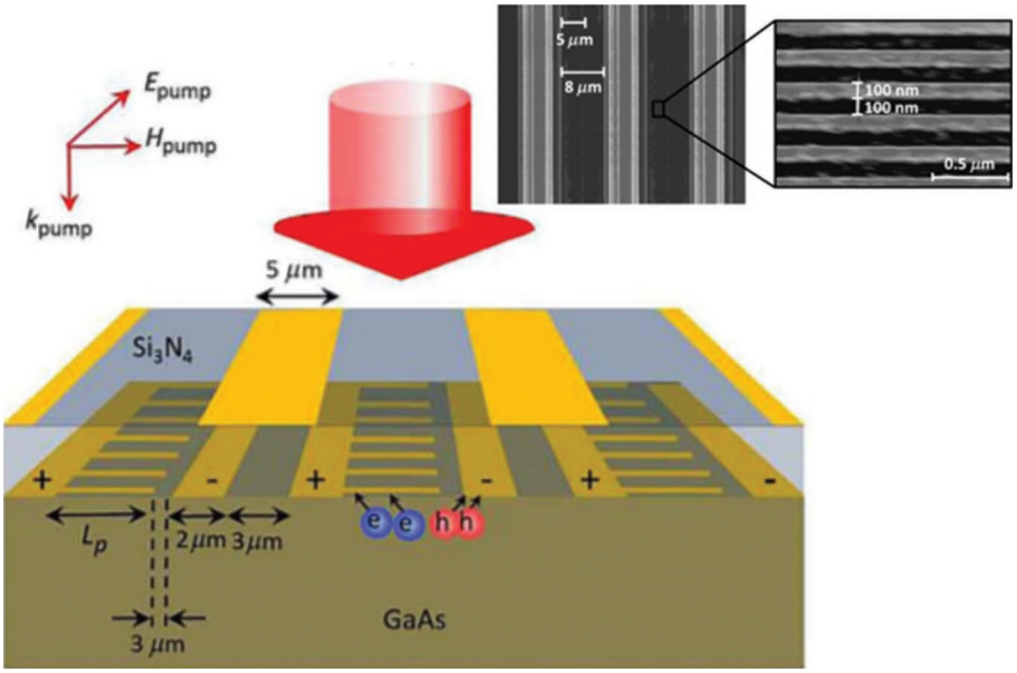

Fig. 12 A photoconductive antenna with contact electrodes for decreasing the path between the two electrodes and SEM image of the fabricated device. Figure retrieved from Ref. 180 with permission from AIP.

was demonstrated through this architecture.[174] As of 2017, the best signal to noise ratio achieved for THz TDS using this architecture was reported to be 107 dB over the 0.1- to 4-THz range of frequency.[175]

In 2019, a multinational research consortium from the United States, Russia, and Japan reported that current–voltage measurements under femtosecond laser illumination show an increase of the transient photocurrent of 15 times higher than that of conventional photoconductive antennas. In terms of THz power spectra, a 100 times increase of the THz power is observed in the reported results as well.[176]

Figure 13 illustrates a design for a THz photoconductive antenna with a channel that includes nanocavities and distributed Bragg reflectors (DBRs).[177] Both nanocavities and DBRs contribute to the enhancement in the percentage of absorbed photons by the active region of the THz photoconductive antenna. As illustrated in Fig. 13, the DBR is fabricated under the active channel of the antenna and reflects back to the active region the photons with a frequency that is within the photonic stopband. To increase the number of absorbed THz photons on the detector side, the DBR is designed to have a stopband in the range of the wavelength of the incident THz photons. On top of the DBR, a gold nanoantenna array is fabricated. As a result of this architecture, the incident photons within the stopband of DBR are trapped (reflected back and forth) in the active region until they are absorbed and thus contribute to the photocurrent. Of course, some portions of the photons escape the trap or are absorbed by parts of the device where they cannot contribute to the photocurrent. Nonetheless, a significant portion of the trapped photons is absorbed in the active region. Hence, this architecture enhances the photo-efficiency of the system significantly. Accordingly, 4 mW over 01- to 5-THz frequency range was reported as the power of the THz radiation through this architecture. This radiation power is 20 times higher than a similarly large area plasmonic LT-GaAs THz emitter without optical nanocavities and DBR.[177–179]

In another research work, an improved design for THz photoconductive antennas was proposed; it features a deep trench in the substrate between electrical pads and a closed-loop junction, which reduces the parasitic capacitance and series resistance, respectively. Based on this modeling approach, a parametric study is carried out to investigate the relationship between the physical parameters of the diode and parasitic elements, which limit the device cutoff frequency.[180]

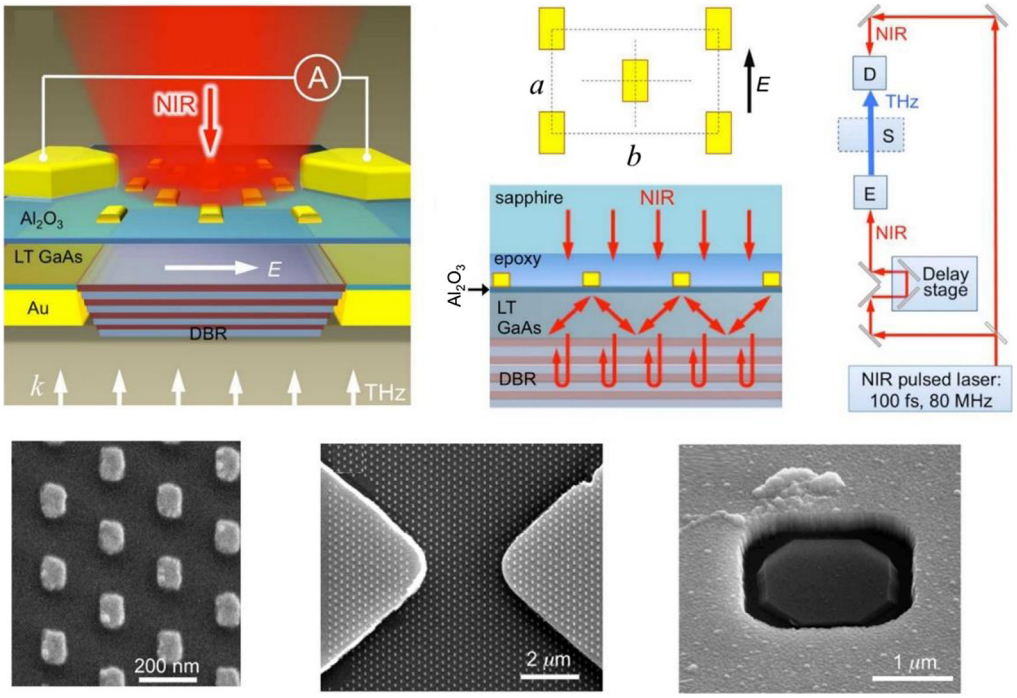

Fig. 13 Optical nanocavities and DBR. The SEM images left to right illustrate gold antenna array, the active region of the THz detector showing two metallic electrodes and the nanoantenna array in the PC gap; a 2-μm square input aperture in the gold screen of the near-field THz probe. Figure retrieved from Ref. 177 with permission from the American Chemical Society.

In addition to the abovementioned designs for enhancing the photon density and frequency of THz radiation, innovative designs for shaping the spectrum of the THz radiation through frequency-dependent impedance modulation have also been proposed.[181,182] Such designs are implemented by altering the electrodes of the photoconductive THz antennas, as outlined in Fig. 14.

In terms of characterization methods of THz photoconductive antennas, Topalli et al.[183] presented an indirect impedance characterization method for planar THz antennas monolithically integrated with electronic sensor devices. This method is based on coplanar contact-probe measurements taken at an accessible location (e.g., a readout pad), which provides crucial experimental data to verify the impedance seen by the integrated device.

3.2 *Advances in Terms of Materials*

Large bandgap semiconductor materials have proven to be promising semiconductor materials for achieving THz devices with higher photon frequencies and emission powers. Among these materials, GaN and GaAs have been the most favorable materials. The first use of GaN for THz application was reported in 1997 in an AIGaN/GaN THz radiation sensor heterostructure field-effect transistor (HFET).[184] The bandgap energy, saturation velocity, and thermal conductivity of GaN are all more than twice that of GaAs. As a result, GaN devices offer higher output power and operation frequency compared with other conventional III to V devices. The mentioned characteristics of GaN together with its capabilities of providing high 2-D electron densities and high longitudinal-optical (LO) phonon of ~90 meV make it one of the most promising semiconductors for the future of generation, detection, mixing, and frequency multiplication of electromagnetic waves in the THz frequency regime.[185] Researchers have proposed and fabricated several innovative GaN-based THz devices, such as GaN-based plasma THz HFETs,[184,186–188] negative differential resistance diode oscillators,[189–191] heterodimensional Schottky diodes,[192,193] impact avalanche transit-time diodes,[194,195] planar Gunn diode,[196] antenna-coupled field-effect transistors,[196–201] THz power radiators based on the Volterra–Wiener

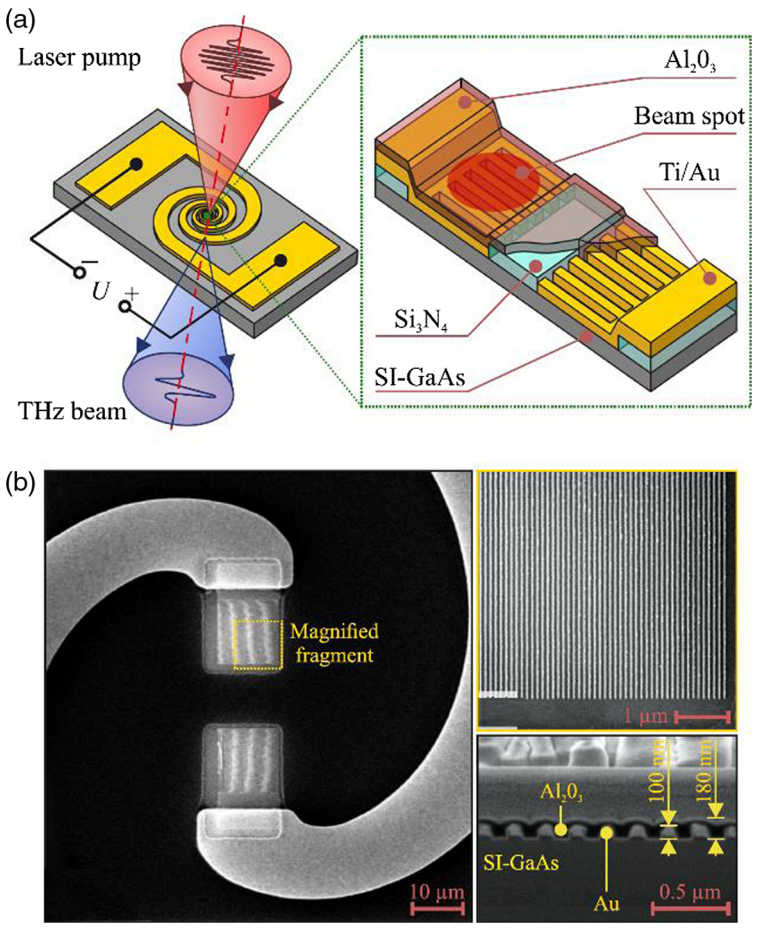

Fig. 14 (a) Schematic of the photoconductive antenna design for modulating THz radiation and (b) a microscopic image of the antenna's arms with its gap. Figure retrieved from Ref. 182 with permission from AIP.

theory of nonlinear systems with frequencies,[202] high electron mobility transistors,[203–205] and QCLs.[206–219] GaN-based devices can fundamentally improve the resolution by enabling THz imaging systems with frequencies higher than 5 THz through enhancing the photon intensity. For instance, GaN-based QCLs can operate in the 5- to 12-THz range[213] whereas operation of conventional naturally cooled GaAs-based QCLs in the upper THz frequency band is limited by a LO phonon of 36 meV.[220]

Table 1 provides the numerical values of the characteristics of GaN and GaAs. The bandgap energy, E_g, saturation velocity, and thermal conductivity of GaN are all more than twice that of GaAs. As a result, GaN devices offer higher output power and operation frequency compared with other conventional III–V devices.[221–224]

Table 1 Comparison between GaN and GaAs and material critical frequencies of operation. Updated and reprinted from Ref. 185, with permission of SPIE.

	Bandgap energy (E_g)		Critical field (E_{CR})	Saturation velocity (V_{SAT})		Thermal conductivity
GaN ✓	3.4 (eV)		2 (MV/cm)	2×107 (cm/s)		1.3 (W/cm)
GaAs	1.4 (eV)		0.4 (MV/cm)	1×107 (cm/s)		0.5 (W/cm)
Material	Si (300 K)	Si (77 K)	GaAs (300 K)	GaAs (77 K)	GaN (300 K)	GaN (77 K)
ω_{cr} (THz)	1.7	0.46 ✗	3.5	0.093 ✗	10 ✓	1.6 ✓

The fundamental plasma frequency is given as

$$\omega_0 = \frac{\pi s}{2L}, \tag{1}$$

where L is the length of the channel and s is the speed of propagation. In a field-effect transistor, eigenmodes of the plasma oscillations are odd harmonics of the fundamental plasma frequency. Thus, for HFET to operate in plasma mode, the length of the channel needs to be limited by the following condition.

$$L \ll L_{\mathrm{cr}} = \frac{s\mu m}{r}, \tag{2}$$

where μ is mobility in low field and m is the effective mass of the electron. This condition is satisfied when

$$\omega_0 \tau \gg 1, \tag{3}$$

where τ is the momentum relaxation time. Consequently, the frequency of operation, ω_{cr}, needs to be much higher for HFET to work in plasma mode:

$$\omega_{\mathrm{cr}} = \frac{1}{\tau}. \tag{4}$$

As indicated in Table 1, ω_{cr} is in the THz regime for GaN for the entire temperature of the operation range.[225]

As illustrated in Fig. 15, plasmonic GaN-based HFETs and QCLs have capabilities of operating in the upper THz frequency band of 5 to 12 THz, at room temperature, and with relatively high emission powers.[219,226–228] According to the studies by the research group of Paiella and Moustakas at Boston University (Fig. 15), the population inversion and consequently the gain coefficient of the GaN/AlGaN quantum wells (QWs) dependence on the temperature are three times smaller than that of GaAs/AlGaAs for THz emission. Moreover, the gain coefficient of the nitride device remains large enough for laser action even without cryogenic cooling.[214–216] As a result, GaN-based devices can operate in the upper THz frequency of 5 to 10 THz at room temperature, which is inaccessible by GaAs-based devices.[213] In 2003, pioneering works reported THz emission from InGaN/GaN multiple QWs.[217,218] In 2015, THz QCLs were fabricated via radiofrequency molecular beam epitaxy and a metal–organic chemical vapor deposition (MOCVD) on MOCVD-growth AlGaN/AlN templates grown on c-plane sapphire substrates. The number of active regions and wave functions, contributing to lasing, were limited to be two QWs and three sub-band levels, respectively. As a result, lasing at ~5.5 and ~7.0 THz was achieved, which was the highest reported emissions for THz QCLs in 2015.[208,213,219] In 2016, researchers from Boston University reported photocurrent peaks near 10 THz for THz intersubband photodetectors, which are developed based on GaN/AlGaN QWs grown on a free-standing semipolar GaN substrate.[211] The photocurrent spectrum and conduction-band lineup of the semipolar GaN/AlGaN QW infrared photodetector developed by this research group are shown in Fig. 15(e). In the latter work, the selective injection into the upper lasing level and a wide dynamic range of operating current density are realized to achieve a higher operating temperature of the THz QCL. The highest reported operation temperature for GaAs/AlGaAs is 160 K for a 1.9-THz QCL and 150 K for a 3.8-THz QCL, whereas GaN-based QCLs can work at room temperature.[229–231] AlGaN/GaN QWs were also proposed for absorption of THz radiation.[232] Reduction in Al mole fraction causes the QW width to increase; thus intersubbands transitions in these QWs are adjustable to be between 1.0 and 10 μm.[209] For absorption in the THz frequency range, plasma-assisted molecular beam epitaxy with tunable absorption from 53 to 160 μm (with respect to doping level and geometrical variations) was reported.[210] A new method for generating THz radiation by exposure to femtosecond laser pulses on the semiconductor surface based on the transverse Dember cross effect was proposed in Refs. 233 and 234.

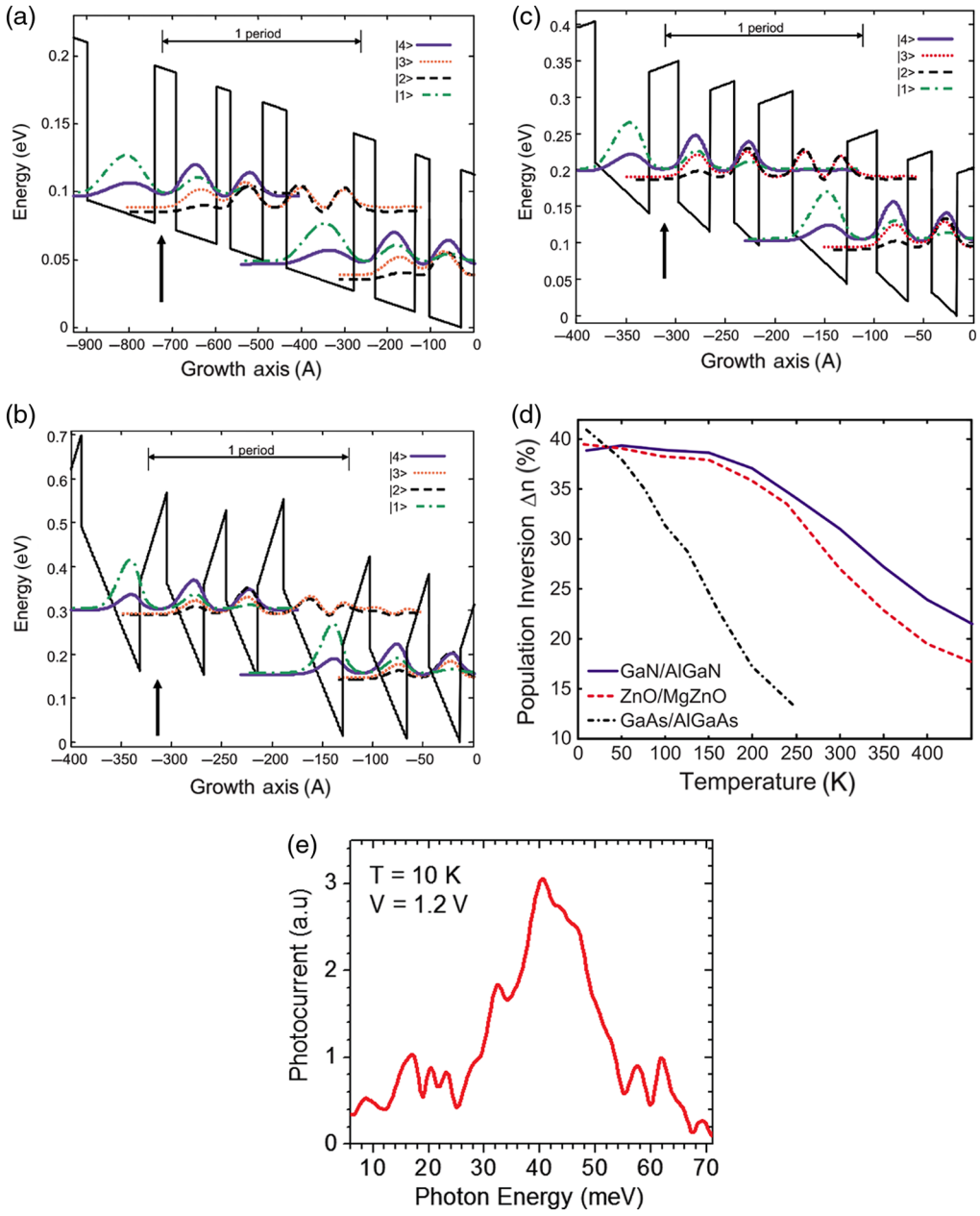

Fig. 15 Conduction-band profile and squared envelope functions of (a) the GaAs/Al0. 15Ga0.85As, (b) the GaN/Al0.15Ga0.85N, and (c) the ZnO/Mg0.15Zn0.85O QC gain media considered in this study. (d) Calculated fractional population inversion of the THz QC structures of (a) (dash-dot line), (b) (solid line), and (c) (dashed line), as a function of temperature. Reprinted from Ref. 214, with permission of AIP. (e) Photocurrent spectrum measured at 10 K under an applied voltage of 1.2 V. Reprinted from Ref. 211 with permission of AIP.

4 Advances in Terahertz Optics, Image Processing, and Data Science

4.1 *Terahertz Optics*

Super resolution can be achieved in near-field THz imaging.[235] However, in near-field imaging systems, objects must be placed at a subwavelength distance from the aperture. Thus, transmission imaging of objects that are thicker than roughly a 100 μm is not possible in near-field THz imaging.[21,236,237] As a result, in most of the applications, near-field THz imaging cannot replace far-field THz imaging. For this reason, a tremendous amount of research is dedicated to the

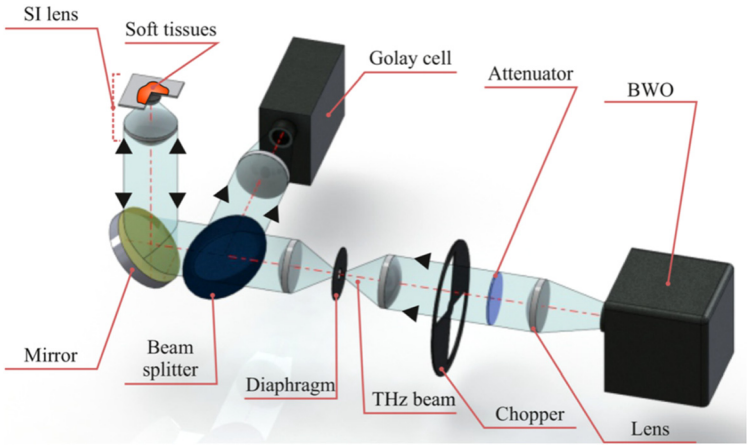

Fig. 16 Schematic of the THz solid immersion microscope for CW reflection-mode imaging of soft tissues. Reprinted from Ref. 247 with permission of AIP.

enhancement of far-field THz imaging. In addition to digital image reconstruction techniques,[238–240] high-resolution THz imaging based on utilizing aperture synthesis,[241] dielectric cube terajet generation,[242–246] solid immersion imaging,[247–250] confocal THz laser microscope,[251] and wide-aperture spherical lens[252,253] for 3-D and flat diffractive optics[254,255] were proposed.

Minins et al. demonstrated that a mesoscale dielectric cube can be exploited as a resolution enhancer by placing it at the focused imaging point of a CW THz imaging system. Using the enhancer at 125 GHz in the THz imaging system, they successfully obtained a diffraction-limited FWHM corresponding to 275 GHz, a 2.2 times higher frequency, without changing the design of the imaging system.[256,257] In 2018 and 2019, researchers from A.M. Prokhorov General Physics Institute demonstrated a 0.15λ resolution of the proposed imaging modality at $\lambda = 500$ μm, which is beyond the Abbe diffraction limit and represents a considerable improvement over the previously reported arrangements of solid immersion imaging setups. The proposed technique does not involve any subwavelength near-field probes and diaphragms; thus, it avoids the THz beam attenuation due to such elements.[247,258] The mentioned work has been demonstrated to be promising for microscopy of soft biological tissues.[259] The schematic of the THz solid immersion microscope for CW reflection-mode imaging of soft tissues is illustrated in Fig. 16.

4.2 *Digital Image Processing and Data Science*

Image reconstruction techniques improve the resultant images of the optics-based resolution-enhancement techniques even further, and thus developments in both areas need to be pursued in parallel. In addition, since THz imaging is fairly a new science, theories and mathematical models for describing the THz imaging systems are not matured yet. Advancing the research and development in THz optics and image reconstruction cannot be done efficiently without well-developed cohesive models and theories.

Stantchev et al.[21] proposed a near-field THz imaging of hidden objects using a single-pixel detector. However, as mentioned in the previous section, the drawback of near-field imaging is the fact that objects thicker than a few hundred micrometers cannot be imaged. Trofimov et al. realized conventional image processing techniques to increase the quality of THz imaging systems.[239,260] Kulya et al. proposed taking material dispersion into account to enhance the quality of THz images.[261] For suppressing the absorption in the physical lenses, diffraction lenses with low absorptions were proposed.[262–265] Ahi et al. developed a mathematical algorithm to incorporate the THz imaging features into the Gaussian beam theory to model the THz point spread function and demerge the subresolution features through deconvolution.[8,266,267] Signal processing and suppression of diffraction through filtering out the delayed beams have also proved significant enhancements in THz images.[268] A software system for automation of the implementation of the high-resolution THz imaging theory of Ref. 268 was also proposed.[269] The user interface of this system is shown in Fig. 17. Kannegulla and Cheng proposed

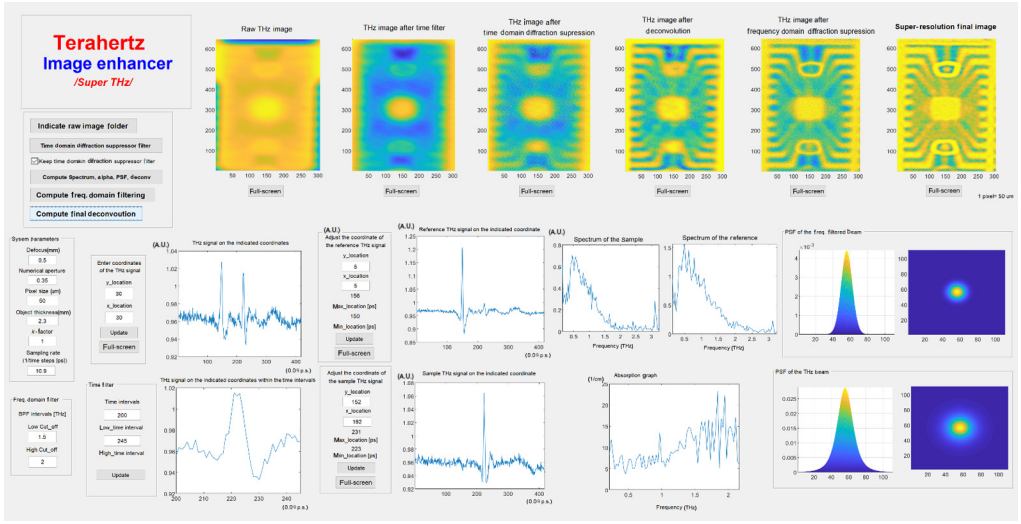

Fig. 17 User interface of an automation software program for implementation of the computational image resolution enhancement theory reported in Ref. 268. The sample is a packaged IC.

subwavelength focusing using hyperbolic metamaterials for enhancement of the THz imaging systems.[270] As illustrated in Fig. 18, the resolution of THz imaging can be enhanced through the reconstruction of the image in THz pulse time-domain holography.[271] Such research can be classified as a numerical approach for increasing the resolution of retrieved images of objects after their diffraction patterns are recorded via THz pulse time-domain holography.

Data postprocessing methods in this field open up the possibility of reconstructing holograms recorded with spatially restricted THz detectors and overcoming the diffraction limit even for the

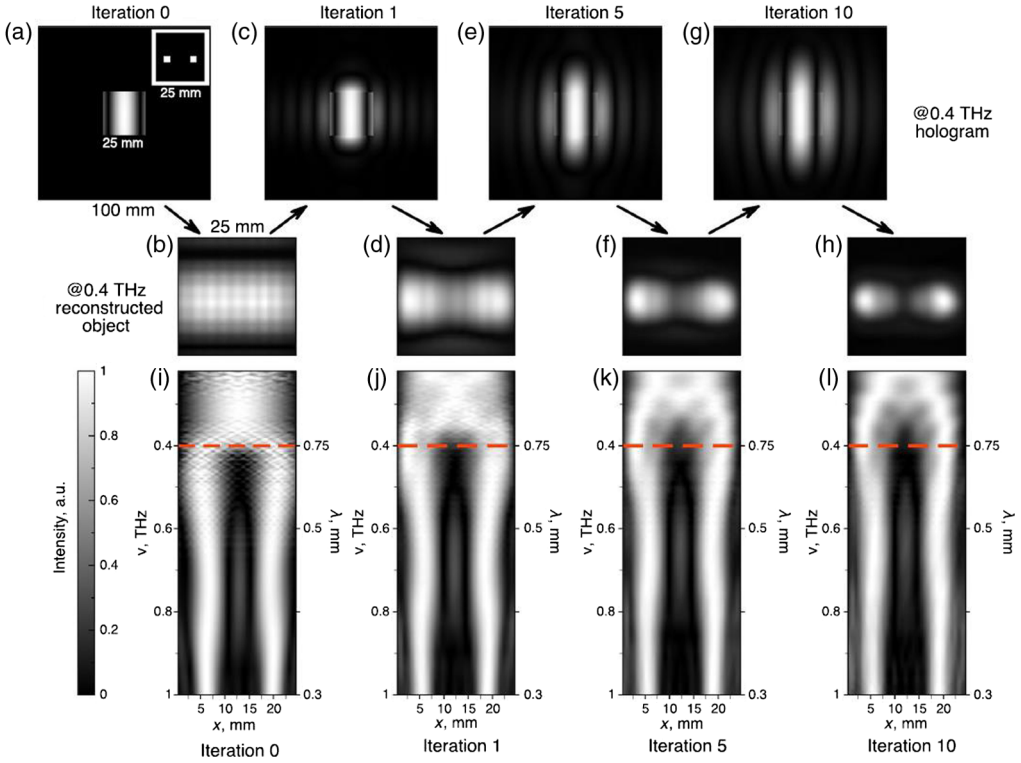

Fig. 18 Resolution enhancement through broadband THz pulse time-domain holography. Reprinted from Ref. 271 with permission of Nature Publication.

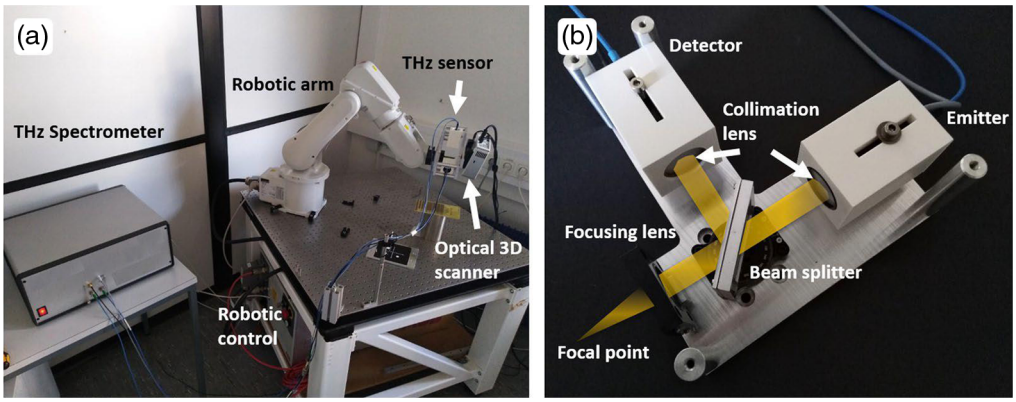

Fig. 19 (a) Overview of the robotic-based THz system and (b) photo of the THz sensor head, including a sketch of the THz beam path. Reprinted from Ref. 277 with permission of Nature Publication.

lower-frequency spectral components.[272] In addition to resolution enhancement, a combination of temporal and complex-domain filters allows for expansion of the dynamic range of THz frequencies. This means that amplitude/phase information as a result of utilizing holography[273] can also be obtained. As the speed of measurement and size of data are becoming more of a critical factor in the successful industrialization of any new technology, comprehensive sampling is attracting more attention.[274] In this respect, research shows that THz imaging can benefit from comprehensive sampling without significant loss in the useful data.[275,276]

4.3 *Automation of Terahertz Imaging and Inspection*

As new applications for THz imaging and inspection are being proposed, the automation of these applications through software programs and robotics becomes more appealing. Biological and medical applications are certainly among the fields in which automation can contribute to the expansion of the THz footprint. In this respect, a robotic THz imaging system for subsurface analysis of ancient human remains was proposed, as shown in Fig. 19.[277,278] The advantage of this system over the conventional computed tomography scan is that THz provides higher depth resolution and is noninvasive.[277]

5 Conclusion and Future Roadmap

THz analysis has progressed by leaps and bounds since the inception of practical wave generation in the 1990s. The first systems were capable of qualitative biophotonic analysis, mostly focused on detecting the presence or absence of water in a sample. However, once higher power output and greater efficiency were achieved, THz analyzers could exploit TDS and frequency analysis to uniquely characterize material profiles. As a result, a drastic number of biomedical applications developed, including imaging opaque samples, performing crop analyses, locating malformed or anomalous tissue samples, identifying defective bone samples, and chemical analysis.

As noted, these functions would not be possible without developments in the generation and capturing of THz frequency waves. Photoconductive antennas greatly increased the number of THz-frequency photons transferring out of the emitter, and the dual nature of this structure also increased the efficiency when operating as a receiver. Multiple parameters affect the operation of these antennas, and they can be tuned to the needs and capabilities of individual researchers. Simultaneous developments were also required in the semiconductor side of photon emission. After all, higher power outputs require more robust hardware to withstand the increased number of incident photons. GaN and GaAs substrates prove promising in this regard. Though these appeared as early as the 1990s, only recent developments in transistors, oscillators, and lasers could fully utilize the capabilities of these unique materials.

Unfortunately, these newly reached THz boundaries are ahead of their image and optical processing counterparts. While some applications are certainly possible with current technology, researchers are still looking into methods of improving far-field imaging techniques and overcoming inherent resolution limitations. These advances arrive by way of innovative devices and mathematical implementations. Such developments include alternative lenses, aperture synthesis, dielectric focusing material, unique point spread beam models, and holographic reconstruction, among others. Combined, these updates in THz technology allow for unprecedented analysis in terms of speed and complexity.

References

1. M. van Exter and D. R. Grischkowsky, "Characterization of an optoelectronic terahertz beam system," *IEEE Trans. Microwaves Theory Tech.* **38**, 1684–1691 (1990).
2. D. M. Mittleman et al., "T-ray tomography," *Opt. Lett.* **22**(12), 904 (1997).
3. K. Ahi, S. Shahbazmohamadi, and N. Asadizanjani, "Quality control and authentication of packaged integrated circuits using enhanced-spatial-resolution terahertz time-domain spectroscopy and imaging," *Opt. Lasers Eng.* **104**, 274–284 (2018).
4. Z. Ali and B. Florent, "Potential of chipless authentication based on randomness inherent in fabrication process for RF and THz," in *Conf. 11th Eur. Conf. Antennas Propag.* (2017).
5. K. Ahi and M. Anwar, "A novel approach for enhancement of the resolution of terahertz measurements for quality control and counterfeit detection," in *Diminishing Manuf. Sources Mater. Shortages*, Phoenix, Arizona (2015).
6. B. Yousefi et al., "Low-rank sparse principal component thermography (sparse-PCT): comparative assessment on detection of subsurface defects," *Infrared Phys. Technol.* **98**, 278–284 (2019).
7. I. S. Gregory et al., "Continuous-wave terahertz system with a 60 dB dynamic range," *Appl. Phys. Lett.* **86**, 204104 (2005).
8. K. Ahi and M. Anwar, "Developing terahertz imaging equation and enhancement of the resolution of terahertz images using deconvolution," *Proc. SPIE* **9856**, 98560N (2016).
9. P. Lopato and T. Chady, "Terahertz detection and identification of defects in layered polymer composites and composite coatings," *Nondestruct. Test. Eval.* **28**, 28–43 (2013).
10. N. S. Balbekin et al., "Nondestructive monitoring of aircraft composites using terahertz radiation," *Proc. SPIE* **9448**, 94482D (2015).
11. T. Hagelschuer et al., "High-spectral-resolution terahertz imaging with a quantum-cascade laser," *Opt. Express* **24**, 13839–13849 (2016).
12. E. V. Yakovlev et al., "Non-destructive evaluation of polymer composite materials at the manufacturing stage using terahertz pulsed spectroscopy," *IEEE Trans. Terahertz Sci. Technol.* **5**, 810–816 (2015).
13. M. Kato et al., "Non-destructive drug inspection in covering materials using a terahertz spectral imaging system with injection-seeded terahertz parametric generation and detection," *Opt. Express* **24**, 6425 (2016).
14. U. Schmidhammer and P. Jeunesse, "Pulsed THz imaging for non-destructive testing of adhesive bonds," in *39th Int. Conf. Infrared, Millimeter, Terahertz Waves*, IEEE, p. 1–2 (2014).
15. X. Neiers, P. Jeunesse, and U. Schmidhammer, "Rapid control of machined glass fiber reinforced plastics by single shot terahertz time domain spectroscopy," in *40th Int. Conf. Infrared, Millimeter, Terahertz Waves*, IEEE, Vol. 13, p. 1–2 (2015).
16. K. Ahi and M. Anwar, "Modeling of terahertz images based on x-ray images: a novel approach for verification of terahertz images and identification of objects with fine details beyond terahertz resolution," *Proc. SPIE* **9856**, 985610 (2016).
17. K. Ahi et al., "Terahertz characterization of electronic components and comparison of terahertz imaging with x-ray imaging techniques," *Proc. SPIE* **9483**, 94830K (2015).
18. V. P. Wallace et al., "Three-dimensional imaging of optically opaque materials using nonionizing terahertz radiation," *J. Opt. Soc. Am. A* **25**, 3120 (2008).

19. J. B. Perraud et al., "Terahertz imaging and tomography as efficient instruments for testing polymer additive manufacturing objects," *Appl. Opt.* **55**, 3462–3467 (2016).
20. H. Balacey et al., "Advanced processing sequence for 3-D THz imaging," *IEEE Trans. Terahertz Sci. Technol.* **6**, 191–198 (2016).
21. R. I. Stantchev et al., "Noninvasive, near-field terahertz imaging of hidden objects using a single-pixel detector," *Sci. Adv.* **2**, e1600190 (2016).
22. F. Rutz et al., "Terahertz quality control of polymeric products," *Int. J. Infrared Millimeter Waves* **27**, 547–556 (2006).
23. K. Ahi and M. Anwar, "Advanced terahertz techniques for quality control and counterfeit detection," *Proc. SPIE* **9856**, 98560G (2016).
24. H. Zhang et al., "An infrared-induced terahertz imaging modality for foreign insert detection in a glass fiber-skinned lightweight honeycomb composite panel," *IEEE Trans. Ind. Inf.* 1–1 (2018).
25. I. Taraghi et al., "X-ray and terahertz imaging as non-destructive techniques for defects detection in nanocomposites foam-core sandwich panels containing carbon nanotubes," *Polym. Test.* **79**, 106084 (2019).
26. M. Kowalski, "Real-time concealed object detection and recognition in passive imaging at 250 GHz," *Appl. Opt.* **58**, 3134 (2019).
27. V. A. Trofimov et al., "New algorithm for detection of dangerous objects hidden on a human body using passive THz camera," *Proc. SPIE* **9993**, 999305 (2016).
28. V. A. Trofimov et al., "Concealed object detection using the passive THz image without its viewing," *Proc. SPIE*, **9830**, 98300E (2016).
29. I. N. Dolganova et al., "A hybrid continuous-wave terahertz imaging system," *Rev. Sci. Instrum.* **86**, 113704 (2015).
30. M. Kowalski and M. Kastek, "Comparative studies of passive imaging in terahertz and mid-wavelength infrared ranges for object detection," *IEEE Trans. Inf. Forensics Secur.* **11**, 2028–2035 (2016).
31. M. Kowalski et al., "Passive imaging of concealed objects in terahertz and long-wavelength infrared," *Appl. Opt.* **54**, 3826 (2015).
32. M. Kowalski, "Hidden object detection and recognition in passive terahertz and mid-wavelength infrared," *J. Infrared, Millimeter, Terahertz Waves* **40**, 1074–1091 (2019).
33. B. Yousefi et al., "Thermography data fusion and nonnegative matrix factorization for the evaluation of cultural heritage objects and buildings," *J. Thermal Anal. Calorimetry* **136**, 943–955 (2019).
34. K. Krügener et al., "Terahertz meets sculptural and architectural art: evaluation and conservation of stone objects with T-ray technology," *Sci. Rep.* **5**, 14842 (2015).
35. K. Krügener et al., "Non-destructive analysis of material detachments from polychromatically glazed terracotta artwork by THz time-of-flight spectroscopy," *J. Infrared, Millimeter, Terahertz Waves* **38**, 495–502 (2017).
36. H. Zhang et al., "Non-destructive investigation of paintings on canvas by continuous wave terahertz imaging and flash thermography," *J. Nondestruct. Eval.* **36**, 34 (2017).
37. K. Krügener et al., "THz tomography for detecting damages on wood caused by insects," *Appl. Opt.* **58**, 6063 (2019).
38. I. N. Dolganova et al., "Nanoparticle-enabled experimentally trained wavelet-domain denoising method for optical coherence tomography," *J. Biomed. Opt.* **23**, 091406 (2018).
39. B. Ferguson et al., "T-ray computed tomography," *Opt. Lett.* **27**, 1312 (2002).
40. N. Rothbart et al., "Fast 2-D and 3-D terahertz imaging with a quantum-cascade laser and a scanning mirror," *IEEE Trans. Terahertz Sci. Technol.* **3**, 617–624 (2013).
41. M. W. Ayech and D. Ziou, "Terahertz image segmentation using k-means clustering based on weighted feature learning and random pixel sampling," *Neurocomputing* **175**, 243–264 (2016).
42. H. Zhang et al., "Numerical and experimental analyses for natural and non-natural impacted composites via thermographic inspection, ultrasonic C-scan and terahertz imaging," *Proc. SPIE* **10214**, 102140I (2017).
43. P. Lopato, "Pulsed excitation terahertz tomography—multiparametric approach," *Open Phys.* **16**, 111–116 (2018).

44. B. M. Giuliano et al., "Broadband spectroscopy of astrophysical ice analogs. I. Direct measurement of complex refractive index of CO ice using terahertz time-domain spectroscopy," ArXiv E-Prints, https://arxiv.org/abs/1907.11491 (2019).
45. P. Knobloch et al., "Medical THz imaging: an investigation of histo-pathological samples," *Phys. Med. Biol.* **47**, 3875–3884 (2002).
46. O. A. Smolyanskaya et al., "Glycerol dehydration of native and diabetic animal tissues studied by THz-TDS and NMR methods," *Biomed. Opt. Express* **9**, 1198 (2018).
47. O. A. Smolyanskaya et al., "Terahertz biophotonics as a tool for studies of dielectric and spectral properties of biological tissues and liquids," *Prog. Quantum Electron.* **62**, 1–77 (2018).
48. A. A. Gavdush et al., "Terahertz spectroscopy of gelatin-embedded human brain gliomas of different grades: a road toward intraoperative THz diagnosis," *J. Biomed. Opt.* **24**, 027001 (2019).
49. O. A. Smolyanskaya et al., "Multimodal optical diagnostics of glycated biological tissues," *Biochemistry* **84**, 124–143 (2019).
50. E. A. Strepitov et al., "Analysis of spectral characteristics of normal fibroblasts and fibroblasts cultured with cancer cells in terahertz frequency range," in *Prog. Electromagn. Res. Symp. Proc.*, pp. 1707–1710 (2014).
51. M. V. Duka et al., "Numerical and experimental studies of mechanisms underlying the effect of pulsed broadband terahertz radiation on nerve cells," *Quantum Electron.* **44**, 707–712 (2014).
52. K. I. Zaytsev et al., "*In vivo* terahertz spectroscopy of pigmentary skin nevi: pilot study of non-invasive early diagnosis of dysplasia," *Appl. Phys. Lett.* **106**, 053702 (2015).
53. K. I. Zaytsev et al., "Highly accurate *in vivo* terahertz spectroscopy of healthy skin: variation of refractive index and absorption coefficient along the human body," *IEEE Trans. Terahertz Sci. Technol.* **5**, 817–827 (2015).
54. M. H. Arbab et al., "Terahertz spectroscopy for the assessment of burn injuries *in vivo*," *J. Biomed. Opt.* **18**, 077004 (2013).
55. M. H. Arbab et al., "Terahertz reflectometry of burn wounds in a rat model," *Biomed. Opt. Express* **2**, 2339 (2011).
56. K. I. Zaytsev et al., "Invariant embedding technique for medium permittivity profile reconstruction using terahertz time-domain spectroscopy," *Opt. Eng.* **52**, 068203 (2013).
57. Z. J. Thompson et al., "Terahertz-triggered phase transition and hysteresis narrowing in a nanoantenna patterned vanadium dioxide film," *Nano Lett.* **15**, 5893–5898 (2015).
58. P. Lopato, "Estimation of layered materials dielectric parameters using pulsed terahertz technique," *Int. J. Appl. Electromagn. Mech.* **43**, 161–168 (2013).
59. K. Kawase et al., "Non-destructive terahertz imaging of illicit drugs using spectral fingerprints," *Opt. Express* **11**, 2549 (2003).
60. H. Zhang et al., "Terahertz image improvement for an environmentally friendly sandwich structure," in *Can. Conf. Electr. Comput. Eng.*, IEEE (2018).
61. H. Zhang et al., "Terahertz amplitude polynomial principle component regression for aramid-basalt hybrid composite laminate inspection," *IEEE Trans. Ind. Inf.* **14**, 5601–5609 (2018).
62. A. O. Chulkov et al., "Evaluating thermal properties of sugarcane bagasse-based composites by using active infrared thermography and terahertz imaging," *Infrared Phys. Technol.* **97**, 432–439 (2019).
63. J. Dong, A. Locquet, and D. S. Citrin, "Depth resolution enhancement of terahertz deconvolution by autoregressive spectral extrapolation," *Opt. Lett.* **42**, 1828 (2017).
64. K. Su, Y.-C. Shen, and J. A. Zeitler, "Terahertz sensor for non-contact thickness and quality measurement of automobile paints of varying complexity," *IEEE Trans. Terahertz Sci. Technol.* **4**, 432–439 (2014).
65. L. Angrisani et al., "First steps towards an innovative compressive sampling based-THz imaging system for early crack detection on aereospace plates," in *IEEE Metrol. Aerosp.*, IEEE, pp. 488–493 (2014).
66. G. P. Papari, C. Koral, and A. Andreone, "Encoded-enhancement of THZ metasurface figure of merit for label-free sensing," *Sensors (Switzerland)* **19**, 2544 (2019).

67. N. S. Balbekin et al., "The modeling peculiarities of diffractive propagation of the broadband terahertz two-dimensional field," *Phys. Procedia* **73**, 49–53 (2015).
68. N. V. Petrov et al., "Application of terahertz pulse time-domain holography for phase imaging," *IEEE Trans. Terahertz Sci. Technol.* **6**, 464–472 (2016).
69. I. V. Il'ina, D. S. Sitnikov, and M. B. Agranat, "State-of-the-art of studies of the effect of terahertz radiation on living biological systems," *High Temp.* **56**, 789–810 (2018).
70. Y. Yeh and V. V. Krishnan, *Introduction to Biophotonics*, Vol. **66** (2018).
71. U. Møller et al., "Terahertz reflection spectroscopy of Debye relaxation in polar liquids [invited]," *J. Opt. Soc. Am. B* **26**, A113 (2009).
72. L. V. Titova et al., "Intense THz pulses cause H2AX phosphorylation and activate DNA damage response in human skin tissue," *Biomed. Opt. Express* **4**, 559 (2013).
73. E. V. Demidova et al., "Impact of terahertz radiation on stress-sensitive genes of *E. coli* cell," *IEEE Trans. Terahertz Sci. Technol.* **6**, 435–441 (2016).
74. L. V. Titova, "Intense THz pulses down-regulate genes associated with skin cancer and psoriasis: a new therapeutic avenue?" *Sci. Rep.* **3**, 1–6 (2013).
75. B. S. Alexandrov et al., "DNA breathing dynamics in the presence of a terahertz field," *Phys. Lett. Sect. A* **374**, 1214–1217 (2010).
76. D. M. Mittleman, "Twenty years of terahertz imaging [invited]," *Opt. Express* **26**, 9417 (2018).
77. B. B. Hu and M. C. Nuss, "Imaging with terahertz waves," *Opt. Lett.* **20**, 1716 (1995).
78. R. Gente and M. Koch, "Monitoring leaf water content with THz and sub-THz waves," *Plant Methods* **11**, 15 (2015).
79. J. H. Son, "Terahertz electromagnetic interactions with biological matter and their applications," *J. Appl. Phys.* **105**, 102033 (2009).
80. R. Sato et al., "Observation of water trees using terahertz spectroscopy and time-domain imaging," *IEEE Trans. Dielectr. Electr. Insul.* **18**, 1570–1577 (2011).
81. N. Born et al., "Monitoring plant drought stress response using terahertz time-domain spectroscopy," *Plant Physiol.* **164**, 1571–1577 (2014).
82. W. Liu et al., "Application of terahertz spectroscopy imaging for discrimination of transgenic rice seeds with chemometrics," *Food Chem.* **210**, 415–421 (2016).
83. Z. Zang et al., "Terahertz spectral imaging based quantitative determination of spatial distribution of plant leaf constituents," *Plant Methods* **15**, 106 (2019).
84. R. Gente et al., "Determination of leaf water content from terahertz time-domain spectroscopic data," *J. Infrared, Millimeter, Terahertz Waves* **34**, 316–323 (2013).
85. C. Jördens, "Detection of foreign bodies in chocolate with pulsed terahertz spectroscopy," *Opt. Eng.* **47**, 037003 (2008).
86. S. K. Mathanker, P. R. Weckler, and N. Wang, "Terahertz (THZ) applications in food and agriculture: a review," *Trans. ASABE* **56**, 1213–1226 (2013).
87. E. Castro-Camus, M. Palomar, and A. A. Covarrubias, "Leaf water dynamics of *Arabidopsis thaliana* monitored *in-vivo* using terahertz time-domain spectroscopy," *Sci. Rep.* **3**, 1–5 (2013).
88. S. J. Oh et al., "Study of freshly excised brain tissues using terahertz imaging," *Biomed. Opt. Express* **5**, 2837 (2014).
89. S. M. Kim et al., "High sensitivity and high selectivity terahertz biomedical imaging," *Chin. Opt. Lett.* **9**, 110009 (2011).
90. C. S. Joseph et al., "Continuous wave terahertz transmission imaging of nonmelanoma skin cancers," *Lasers Surg. Med.* **43**, 457–462 (2011).
91. Q. Sun et al., "Recent advances in terahertz technology for biomedical applications," *Quantum Imaging Med. Surg.* **7**, 345–355 (2017).
92. S. Fan et al., "The growth of biomedical terahertz research," *J. Phys. D Appl. Phys.* **47**, 374009 (2014).
93. R. M. Woodward et al., "Terahertz pulse imaging of *ex vivo* basal cell carcinoma," *J. Invest. Dermatol.* **120**, 72–78 (2003).
94. V. P. Wallace et al., "Terahertz pulsed imaging of basal cell carcinoma *ex vivo* and *in vivo*," *Br. J. Dermatol.* **151**, 424–432 (2004).

95. F. Wahaia et al., "Study of paraffin-embedded colon cancer tissue using terahertz spectroscopy," *J. Mol. Struct.* **1079**, 448–453 (2015).
96. S. W. Smye et al., "The interaction between terahertz radiation and biological tissue," *Phys. Med. Biol.* **46**, R101–R112 (2001).
97. K. Zaytsev et al., "The progress and perspectives of terahertz technology for diagnosis of neoplasms: a review," *J. Opt.* **22**, 013001 (2020).
98. J. A. Kanis et al., "WHO study group on assessment of fracture risk and its application to Screening for post-menopausal osteoporosis: report of a WHO study group (series 843)," in *Ge 2002*, pp. 527–536 (1994).
99. J. Ryu et al., "Diagnosis of dental cavity and osteoporosis using terahertz transmission images," *Springer Ser. Chem. Phys.* **66**, 265–267 (2001).
100. B. A. Knyazev et al., "Using of terahertz radiation for monitoring of senile osteoporosis development," in *IRMMW-THz2007—Conf. Dig. Joint 32nd Int. Conf. Infrared Millimetre Waves, and 15th Int. Conf. Terahertz Electron.*, pp. 563–564 (2007).
101. M. R. Stringer et al., "The analysis of human cortical bone by terahertz time-domain spectroscopy," *Phys. Med. Biol.* **50**, 3211–3219 (2005).
102. M. Bessou et al., "Three-dimensional terahertz computed tomography of human bones," *Appl. Opt.* **51**, 6738–6744 (2012).
103. D. B. Bennett et al., "Terahertz sensing in corneal tissues," *J. Biomed. Opt.* **16**, 057003 (2011).
104. N. Bajwa et al., "*In vivo* confirmation of hydration based contrast mechanisms for terahertz medical imaging using MRI," *Proc. SPIE* **9199**, 91990U (2014).
105. P. Tewari et al., "*In vivo* terahertz imaging of rat skin burns," *J. Biomed. Opt.* **17**, 040503 (2012).
106. A. J. Fitzgerald et al., "Catalogue of human tissue optical properties at terahertz frequencies," *J. Biol. Phys.* **29**, 123–128 (2003).
107. B. E. Cole et al., "Terahertz imaging and spectroscopy of human skin *in vivo*," *Proc. SPIE* **4276**, 1–10 (2001).
108. Y. Sun, "A promising diagnostic method: terahertz pulsed imaging and spectroscopy," *World J. Radiol.* **3**, 55 (2011).
109. E. Berry et al., "Do *in vivo* terahertz imaging systems comply with safety guidelines?" *J. Laser Appl.* **15**, 192–198 (2003).
110. O. P. Cherkasova et al., "Studying human and animal skin optical properties by terahertz time-domain spectroscopy," *Bull. Russ. Acad. Sci. Phys.* **80**, 479–483 (2016).
111. A. Y. Babenko et al., "The dynamics of invasive and noninvasive blood glucose monitoring methods: recent trends," *Diabetes Mellit.* **19**, 397–405 (2016).
112. S. I. Gusev et al., "Study of glucose concentration influence on blood optical properties in THz frequency range," *Nanosyst. Phys., Chem. Math.* **1124**, 389–400 (2018).
113. T. Torii et al., "Measurements of glucose concentration in aqueous solutions using reflected THz radiation for applications to a novel sub-THz radiation non-invasive blood sugar measurement method," *Digit Health* **3**, 205520761772953 (2017).
114. H. Chen et al., "*In vivo* non-invasive diagnosis of glucose level in type-2 diabetes mouse by THz near-field imaging," *J. Infrared, Millimeter, Terahertz Waves* **40**, 456–465 (2019).
115. O. P. Cherkasova et al., "Analysis of blood plasma at terahertz frequencies," *Opt. Spectrosc. (English Transl. Opt i Spektrosk)* **120**, 50–57 (2016).
116. I. Heller et al., "Mobility analysis of super-resolved proteins on optically stretched DNA: comparing imaging techniques and parameters," *ChemPhysChem* **15**, 727–733 (2014).
117. P. H. Bolivar et al., "Label-free probing of the binding state of DNA by time-domain terahertz sensing," *Mater. Sci. Forum* **384–385**, 253–258 (2002).
118. B. M. Fischer, M. Walther, and P. U. Jepsen, "Far-infrared vibrational modes of DNA components studied by terahertz time-domain spectroscopy," *Phys. Med. Biol.* **47**, 3807–3814 (2002).
119. X. Yang et al., "Biomedical applications of terahertz spectroscopy and imaging," *Trends Biotechnol.* **34**, 810–824 (2016).
120. M. Nagel et al., "A functionalized THz sensor for marker-free DNA analysis," *Phys. Med. Biol.* **48**, 3625–3636 (2003).

121. J. T. Kindt and C. A. Schmuttenmaer, "Far-infrared dielectric properties of polar liquids probed by femtosecond terahertz pulse spectroscopy," *J. Phys. Chem.* **100**, 10373–10379 (1996).
122. R. Kopelman and W. Tan, "Near-field optics: imaging single molecules," *Science (80-)* **262**, 1382LP–1384LP (1993).
123. C. Wei et al., "Terahertz irradiation-induced motility enhancement and intracellular calcium elevation in human sperm *in vitro*," *Biomed. Opt. Express* **9**, 3998 (2018).
124. M. Nagel et al., "Integrated THz technology for label-free genetic diagnostics," *Appl. Phys. Lett.* **80**, 154–156 (2002).
125. A. G. Markelz, A. Roitberg, and E. J. Heilweil, "Pulsed terahertz spectroscopy of DNA, bovine serum albumin and collagen between 0.1 and 2.0 THz," *Chem. Phys. Lett.* **320**, 42–48 (2000).
126. T. Globus et al., "THz-frequency spectroscopic sensing of DNA and related biological materials," *Int. J. High Speed Electron. Syst.* **13**, 903–936 (2003).
127. W. E. Moerner, "New directions in single-molecule imaging and analysis," *Proc. Natl. Acad. Sci. U. S. A.* **104**, 12596–12602 (2007).
128. Y. Ogawa et al., "Interference terahertz label-free imaging for protein detection on a membrane," *Opt. Express* **16**, 22083 (2008).
129. D. F. Plusquellic et al., "Applications of terahertz spectroscopy in biosystems," *ChemPhysChem* **8**, 2412–2431 (2007).
130. S. Yamazaki et al., "Actin polymerization is activated by terahertz irradiation," *Sci. Rep.* **8**, 1–7 (2018).
131. Y. Li et al., "A comparative evaluation of the activities of thiol group and hydroxyl group in low-frequency vibrations using terahertz spectroscopy and DFT calculations," *Spectrochim Acta Part A-Mol. Biomol. Spectrosc.* **214**, 246–251 (2019).
132. Z. Zang et al., "Temperature- and pH-dependent protein conformational changes investigated by terahertz dielectric spectroscopy," *Infrared Phys. Technol.* **98**, 260–265 (2019).
133. A. Carpinteri et al., "Terahertz vibration modes in Na/K-ATPase," *J. Biomol. Struct. Dyn.* **37**, 256–264 (2019).
134. S. H. Lu et al., "An effective approach to quantitative analysis of ternary amino acids in foxtail millet substrate based on terahertz spectroscopy," *Food Chem.* **246**, 220–227 (2018).
135. H. Elayan, R. M. Shubair, and J. M. Jornet, "Characterising THz propagation and intra-body thermal absorption in iWNSNs," *IET Microwaves Antennas Propag.* **12**, 525–532 (2018).
136. X. Han et al., "Label-free protein detection using terahertz time-domain spectroscopy," *Biomed. Opt. Express* **9**, 994–1005 (2018).
137. S. P. Thirumuruganandham et al., "Terahertz spectroscopy to determine cold shock protein stability upon solvation and evaporation-a molecular dynamics study," *IEEE Trans. Terahertz Sci. Technol.* **7**, 131–143 (2017).
138. Y. Ueno et al., "Quantitative measurements of amino acids by terahertz time-domain transmission spectroscopy," *Anal. Chem.* **78**, 5424–5428 (2006).
139. K. Yamamoto et al., "Terahertz time-domain spectroscopy of amino acids and polypeptides," *Biophys. J.* **89**, L22–L24 (2005).
140. P. J. Huang et al., "Classification and identification of amino acids based on THz spectroscopy," in *Sel. Proc. from CSOE* (2015).
141. G. M. Png et al., "terahertz spectroscopic differentiation of microstructures in protein gels," *Opt. Express* **17**, 13102 (2009).
142. J. F. de Boer, R. Leitgeb, and M. Wojtkowski, "Twenty-five years of optical coherence tomography: the paradigm shift in sensitivity and speed provided by Fourier domain OCT [Invited]," *Biomed. Opt. Express* **8**, 3248 (2017).
143. D. Hillmann et al., "Common approach for compensation of axial motion artifacts in swept-source OCT and dispersion in Fourier-domain OCT," *Opt. Express* **20**, 6761 (2012).
144. S. Zhong et al., "Non-destructive quantification of pharmaceutical tablet coatings using terahertz pulsed imaging and optical coherence tomography," *Opt. Lasers Eng.* **49**, 361–365 (2011).

145. C. L. K. Dandolo et al., "Toward a multimodal fusion of layered cultural object images: complementarity of optical coherence tomography and terahertz time-domain imaging in the heritage field," *Appl. Opt.* **58**(5), 1281–1290 (2019).
146. T. Ikeou et al., "Terahertz imaging using swept source optical-coherence-tomography techniques," in *IEEE Int. Topical Meeting on Microwave Photonics*, IEEE, Noordwijk, Netherlands, pp. 290–293 (2012).
147. A. W. M. Lee et al., "THz optical coherence tomography based on quantum cascade lasers," in *IRMMW-THz 2011—36th Int. Conf. Infrared, Millimeter, Terahertz Waves*, pp. 1–3 (2011).
148. T. Isogawa et al., "Tomographic imaging using photonically generated low-coherence terahertz noise sources," *IEEE Trans. Terahertz Sci. Technol.* **2**, 485–492 (2012).
149. T. Nagatsuma, T. Ikeo, and H. Nishii, "Terahertz imaging based on optical coherence tomography," in *ICECom 2013—Conf. Proc. 21st Int. Conf. Appl. Electromagn. Commun.*, Vol. 2, pp. 64–69 (2013).
150. A. Fitzgerald et al., "Co-registered combined OCT and THz imaging to extract depth and refractive index of a tissue equivalent test object," *Biomed. Opt. Express* **11**, 1417–1431 (2020).
151. H. Kitahara, M. Tani, and M. Hangyo, "Frequency-domain optical coherence tomography system in the terahertz region," *Appl. Phys. B Lasers Opt.* **126**, 1–6 (2020).
152. S. R. Tripathi et al., "Morphology of human sweat ducts observed by optical coherence tomography and their frequency of resonance in the terahertz frequency region," *Sci. Rep.* **5**, 9071 (2015).
153. T. S. Hartwick et al., "Far infrared imagery," *Appl. Opt.* **15**, 1919 (1976).
154. B. E. A. Saleh and M. C. Teich, *Fundamentals of Photonics*, n.d.
155. B. E. A. Saleh and M. C. Teich, *Fundamentals of Photonics*, 2nd ed., p. 1200, Wiley (2007).
156. N. M. Burford and M. O. El-Shenawee, "Review of terahertz photoconductive antenna technology," *Opt. Eng.* **56**, 010901 (2017).
157. N. T. Yardimci and M. Jarrahi, "Nanostructure-enhanced photoconductive terahertz emission and detection," *Small* **14**, 1802437 (2018).
158. N. T. Yardimci et al., "A high-responsivity and broadband photoconductive terahertz detector based on a plasmonic nanocavity," *Appl. Phys. Lett.* **113**, 251102 (2018).
159. I. V. Gorbenko, V. Y. Kachorovskii, and M. S. Shur, "Plasmonic helicity-driven detector of terahertz radiation," *Phys. Status Solidi—Rapid Res. Lett.* **13**, 1800464 (2019).
160. S.-G. Park et al., "Terahertz photoconductive antenna with metal nanoislands," *Opt. Express* **20**, 25530 (2012).
161. M. Unlu et al., "Switchable scattering meta-surfaces for broadband terahertz modulation," *Sci. Rep.* **4**, 5708 (2014).
162. M. Unlu and M. Jarrahi, "Miniature multi-contact MEMS switch for broadband terahertz modulation," *Opt. Express* **22**, 32245 (2014).
163. M. R. M. Hashemi et al., "Electronically-controlled beam-steering through vanadium dioxide metasurfaces," *Sci. Rep.* **6**, 35439 (2016).
164. A. Hartschuh et al., "High-resolution near-field Raman microscopy of single-walled carbon nanotubes," *Phys. Rev. Lett.* **90**, 4 (2003).
165. A. Jooshesh et al., "Plasmon-enhanced below bandgap photoconductive terahertz generation and detection," *Nano Lett.* **15**, 8306–8310 (2015).
166. C. W. Berry et al., "Significant performance enhancement in photoconductive terahertz optoelectronics by incorporating plasmonic contact electrodes," *Nat. Commun.* **4**, 1622 (2013).
167. C. W. Berry and M. Jarrahi, "Plasmonically-enhanced localization of light into photoconductive antennas," in *Opt. InfoBase Conf. Pap.* (2010).
168. R. Salas et al., "Growth rate and surfactant-assisted enhancements of rare-earth arsenide InGaAs nanocomposites for terahertz generation," *APL Mater.* **5**, 096106 (2017).
169. B. Y. Hsieh and M. Jarrahi, "Analysis of periodic metallic nano-slits for efficient interaction of terahertz and optical waves at nano-scale dimensions," *J. Appl. Phys.* **109**, 084326 (2011).

170. X. Li, N. T. Yardimci, and M. Jarrahi, "A polarization-insensitive plasmonic photoconductive terahertz emitter," *AIP Adv.* **7**, 115113 (2017).
171. A. Dreyhaupt et al., "High-intensity terahertz radiation from a microstructured large-area photoconductor," *Appl. Phys. Lett.* **86**, 121114 (2005).
172. OSA, "Impulsive terahertz radiation with high electric fields from an amplifier-driven large-area photoconductive antenna," (n.d.).
173. O. A. Castañeda-Uribe et al., "Comparative study of equivalent circuit models for photoconductive antennas," *Opt. Express* **26**, 29017 (2018).
174. N. T. Yardimci et al., "Impact of substrate characteristics on performance of large area plasmonic photoconductive emitters," *Opt. Express* **23**, 32035 (2015).
175. N. T. Yardimci and M. Jarrahi, "High sensitivity terahertz detection through large-area plasmonic nano-antenna arrays," *Sci. Rep.* **7**, 42667 (2017).
176. D. Ponomarev et al., "Plasmonic terahertz emitters with high-aspect ratio metal gratings," *Proc. SPIE* **11022**, 1102203 (2019).
177. O. Mitrofanov et al., "Photoconductive terahertz near-field detector with a hybrid nanoantenna array cavity," *ACS Photonics* **2**, 1763–1768 (2015).
178. N. T. Yardimci et al., "A high-power broadband terahertz source enabled by three-dimensional light confinement in a plasmonic nanocavity," *Sci. Rep.* **7**, 4166 (2017).
179. O. Mitrofanov et al., "Efficient photoconductive terahertz detector with all-dielectric optical metasurface," *APL Photonics* **3**, 051703 (2018).
180. A. Ghobadi et al., "A performance-enhanced planar Schottky diode for terahertz applications: an electromagnetic modeling approach," *Int. J. Microwaves Wireless Technol.* **9**, 1905–1913 (2017).
181. D. V. Lavrukhin et al., "Shaping the spectrum of terahertz photoconductive antenna by frequency-dependent impedance modulation," *Semicond. Sci. Technol.* **34**, 34005 (2019).
182. D. V. Lavrukhin et al., "Terahertz photoconductive emitter with dielectric-embedded high-aspect-ratio plasmonic grating for operation with low-power optical pumps," *AIP Adv.* **9**, 015112 (2019).
183. K. Topalli, G. C. Trichopoulos, and K. Sertel, "An indirect impedance characterization method for monolithic THz antennas using coplanar probe measurements," *IEEE Antennas Wireless Propag. Lett.* **11**, 3–5 (2012).
184. J. Q. Lu et al., "Detection of microwave radiation by electronic fluid in AlGaN/GaN heterostructure field effect transistors," in *Proc. IEEE/Cornell Conf. Adv. Concepts High Speed Semicond. Devices Circuits CORNEL-97*, IEEE, p. 211–217 (1997).
185. K. Ahi, "Review of GaN-based devices for terahertz operation," *Opt. Eng.* **56**, 090901 (2017).
186. M. Dyakonov and M. Shur, "Detection, mixing, and frequency multiplication of terahertz radiation by two-dimensional electronic fluid," *IEEE Trans. Electron. Devices* **43**, 380–387 (1996).
187. M. S. Shur and J.-Q. Lu, "Terahertz sources and detectors using two-dimensional electronic fluid in high electron-mobility transistors," *IEEE Trans. Microwaves Theory Tech.* **48**, 750–756 (2000).
188. A. El Fatimy et al., "Terahertz detection by GaN/AlGaN transistors," *Electron. Lett.* **42**, 1342 (2006).
189. I. Kostakis, D. Saeedkia, and M. Missous, "Characterization of low temperature InGaAs-InAlAs semiconductor photo mixers at 1.55 μm wavelength illumination for terahertz generation and detection," *J. Appl. Phys.* **111**, 103105 (2012).
190. E. Alekseev and D. Pavlidis, "GaN Gunn diodes for THz signal generation," in *IEEE MTT-S Int. Microwaves Symp. Digest (Cat No00CH37017)*, Vol. 3, pp. 1905–1908 (2000).
191. E. Alekseev et al., "GaN-based NDR devices for THz generation," in *Int. Symp. Space Terahertz Technol.*, p. 162 (2000).
192. D. Veksler et al., "GaN heterodimensional Schottky diode for THz detection," in *5th IEEE Conf. Sens.*, IEEE, p. 323–326 (2006).
193. W. C. B. Peatman, T. W. Crowe, and M. Shur, "A novel Schottky/2-DEG diode for millimeter- and submillimeter-wave multiplier applications," *IEEE Electron. Device Lett.* **13**, 11–13 (1992).

194. A. Reklaitis, "Monte Carlo study of hot-carrier transport in bulk wurtzite GaN and modeling of a near-terahertz impact avalanche transit time diode," *J. Appl. Phys.* **95**, 7925 (2004).
195. A. Reklaitis and L. Reggiani, "Giant suppression of avalanche noise in GaN double-drift impact diodes," *Solid State Electron.* **49**, 405–408 (2005).
196. Y. Wang et al., "Modulation of the domain mode in GaN-based planar Gunn diode for terahertz applications," *Phys. Status Solidi* **13**, 382–385 (2016).
197. X. Liu and M. Shur, "An efficient TCAD model for TeraFET detectors," in *IEEE Radio Wireless Symp., RWS*, IEEE Computer Society (2019).
198. M. Bauer et al., "High-sensitivity wideband THz detectors based on GaN HEMTs with integrated bow-tie antennas," in *10th Eur. Microwaves Integr. Circuits Conf.*, IEEE, p. 1–4 (2015).
199. S. Boppel et al., "0.25-GaN TeraFETs optimized as THz power detectors and intensity-gradient sensors," *IEEE Trans. Terahertz Sci. Technol.* **6**, 348–350 (2016).
200. R. Han et al., "25.5 A 320GHz phase-locked transmitter with 3.3 mW radiated power and 22.5 dBm EIRP for heterodyne THz imaging systems," in *IEEE Int. Solid-State Circuits Conf.—Digest of Tech. Pap.*, IEEE, Vol. 50, p. 1–3 (2015).
201. R. Han et al., "A SiGe terahertz heterodyne imaging transmitter with 3.3 mW radiated power and fully-integrated phase-locked loop," *IEEE J. Solid-State Circuits* **50**, 2935–2947 (2015).
202. H. Aghasi, A. Cathelin, and E. Afshari, "A 0.92-THz SiGe power radiator based on a nonlinear theory for harmonic generation," *IEEE J. Solid-State Circuits* **52**, 406–422 (2017).
203. J. D. Sun et al., "High-responsivity, low-noise, room-temperature, self-mixing terahertz detector realized using floating antennas on a GaN-based field-effect transistor," *Appl. Phys. Lett.* **100**, 013506 (2012).
204. J. D. Sun et al., "Probing and modelling the localized self-mixing in a GaN/AlGaN field-effect terahertz detector," *Appl. Phys. Lett.* **100**, 173513 (2012).
205. H. Hou et al., "Modelling of GaN HEMTs as terahertz detectors based on self-mixing," *Procedia Eng.* **141**, 98–102 (2016).
206. J. Faist et al., "Quantum cascade laser," *Science (80-)* **264**, 553–556 (1994).
207. R. Köhler et al., "Terahertz semiconductor-heterostructure laser," *Nature* **417**, 156–159 (2002).
208. W. Terashima and H. Hirayama, *Terahertz Frequency Emission with Novel Quantum Cascade Laser Designs*, SPIE, pp. 11–13 (2015).
209. M. Beeler, E. Trichas, and E. Monroy, "III-nitride semiconductors for intersubband optoelectronics: a review," *Semicond. Sci. Technol.* **28**, 074022 (2013).
210. M. Beeler et al., "Pseudo-square AlGaN/GaN quantum wells for terahertz absorption," *Appl. Phys. Lett.* **105**, 131106 (2014).
211. H. Durmaz et al., "Terahertz intersubband photodetectors based on semi-polar GaN/AlGaN heterostructures," *Appl. Phys. Lett.* **108**, 201102 (2016).
212. B. S. Williams et al., "Operation of terahertz quantum-cascade lasers at 164 K in pulsed mode and at 117 K in continuous-wave mode," *Opt. Express* **13**, 3331 (2005).
213. W. Terashima and H. Hirayama, "GaN-based terahertz quantum cascade lasers," *Proc. SPIE* **9483**, 948304 (2015).
214. E. Bellotti et al., "Monte Carlo simulation of terahertz quantum cascade laser structures based on wide-bandgap semiconductors," *J. Appl. Phys.* **105**, 113103 (2009).
215. E. Bellotti et al., "Monte Carlo study of GaN versus GaAs terahertz quantum cascade structures," *Appl. Phys. Lett.* **92**, 101112 (2008).
216. F. Sudradjat et al., "Sequential tunneling transport characteristics of GaN/AlGaN coupled-quantum-well structures," *J. Appl. Phys.* **108**, 103704 (2010).
217. D. Turchinovich et al., "Ultrafast polarization dynamics in biased quantum wells under strong femtosecond optical excitation," *Phys. Rev. B* **68**, 241307 (2003).
218. D. Turchinovich, B. S. Monozon, and P. U. Jepsen, "Role of dynamical screening in excitation kinetics of biased quantum wells: nonlinear absorption and ultrabroadband terahertz emission," *J. Appl. Phys.* **99**, 013510 (2006).
219. H. Hirayama et al., "Recent progress and future prospects of THz quantum-cascade lasers," *Proc. SPIE* **9382**, 938211 (2015).

220. B. Mirzaei, A. Rostami, and H. Baghban, "Terahertz dual-wavelength quantum cascade laser based on GaN active region," *Opt. Laser Technol.* **44**, 378–383 (2012).
221. M. Marso, "GaN for THz sources," in *Conf. Proc.—8th Int. Conf. Adv. Semicond. Devices Microsyst.*, pp. 147–154 (2010).
222. D. Pavlidis, "GaN THz electronics," in *Eur. Gall Arsenide Relat. III-V Compd. Appl. Symp.*, pp. 551–554 (2004).
223. J. Li et al., "Efficient terahertz wave generation from GaP crystals pumped by chirp-controlled pulses from femtosecond photonic crystal fiber amplifier," *Appl. Phys. Lett.* **104**, 1–6 (2014).
224. J. Li et al., "Generation of 0.3 mW high-power broadband terahertz pulses from GaP crystal pumped by negatively chirped femtosecond laser pulses," *Laser Phys. Lett.* **10**, 125404 (2013).
225. M. I. Dyakonov and M. S. Shur, "Plasma wave electronics: novel terahertz devices using two dimensional electron fluid," *IEEE Trans. Electron. Devices* **43**, 1640–1645 (1996).
226. T. Otsuji and M. Shur, "Terahertz plasmonics: good results and great expectations," *IEEE Microwaves Mag.* **15**, 43–50 (2014).
227. M. Shur, "AlGaN/GaN plasmonic terahertz electronic devices," *J. Phys. Conf. Ser.* **486**, 012025 (2014).
228. M. Tonouchi, "Cutting-edge terahertz technology," *Nat. Photonics* **1**, 97–105 (2007).
229. S. Miho, T.-T. Lin, and H. Hirayama, "1.9 THz selective injection design quantum cascade laser operating at extreme higher temperature above the k_BT line," *Phys. Status Solidi* **10**, 1448–14451 (2013).
230. T.-T. Lin and H. Hirayama, "Improvement of operation temperature in GaAs/AlGaAs THz-QCLs by utilizing high Al composition barrier," *Phys Status Solidi* **10**, 1430–1433 (2013).
231. T.-T. Lin, L. Ying, and H. Hirayama, "Threshold current density reduction by utilizing high-Al-composition barriers in 3.7 THz GaAs/AlxGa1-xAs quantum cascade lasers," *Appl. Phys. Express* **5**, 012101 (2012).
232. C. Edmunds et al., "Terahertz intersubband absorption in non-polar m-plane AlGaN/GaN quantum wells," *Appl. Phys. Lett.* **105**, 021109 (2014).
233. I. V. Minin and O. V. Minin, "Multielement emitters of terahertz radiation based on array of photonic jet," in *13th Int. Sci. Conf. Actual Prob. Electron. Instrum. Eng. 2016—Proc.*, Institute of Electrical and Electronics Engineers Inc., Vol. 1, p. 140–141 (2016).
234. I. Minin and O. V. Minin, "Ultrafast all-optical THz modulation based on wavelength scaled dielectric particle with graphene monolayer," *Proc. SPIE* **11065**, 110651J (2019).
235. H.-T. Chen, R. Kersting, and G. C. Cho, "Terahertz imaging with nanometer resolution," *Appl. Phys. Lett.* **83**, 3009 (2003).
236. F. Blanchard et al., "Real-time, subwavelength terahertz imaging," *Annu. Rev. Mater. Res.* **43**, 237–259 (2013).
237. F. Blanchard and K. Tanaka, "Improving time and space resolution in electro-optic sampling for near-field terahertz imaging," *Opt. Lett.* **41**, 4645 (2016).
238. V. A. Trofimov and V. V. Trofimov, "New algorithm for the passive THz image quality enhancement," *Proc. SPIE* **9856**, 98560M (2016).
239. V. A. Trofimov et al., "Increasing the instrumental resolution of a commercially available passive THz camera due to computer treatment of image," in *Proc. 2012 5th Global Symp. Millimeter-Waves*, IEEE, p. 427–430 (2012).
240. V. A. Trofimov, V. V. Trofimov, and I. E. Kuchik, "Resolution enhancing of commercially available passive THz cameras due to computer processing," *Proc. SPIE* **9199**, 91990P (2014).
241. V. Krozer et al., "Terahertz imaging systems with aperture synthesis techniques," *IEEE Trans Microwaves Theory Tech.* **58**, 2027–2039 (2010).
242. I. V. Minin et al., "All-dielectric periodic terajet waveguide using an array of coupled cuboids," *Appl. Phys. Lett.* **106**, 254102 (2015).
243. H. H. Nguyen Pham et al., "Enhancement of spatial resolution of terahertz imaging systems based on terajet generation by dielectric cube," *APL Photonics* **2**, 056106 (2017).

244. I. V. Minin and O. V. Minin, "Terahertz artificial dielectric cuboid lens on substrate for super-resolution images," *Opt. Quantum Electron.* **49**, 326 (2017).
245. L. Yue et al., "Photonic hook: a new curved light beam," *Opt. Lett.* **43**, 771 (2018).
246. I. V. Minin et al., "Experimental observation of a photonic hook," *Appl. Phys. Lett.* **114**, 031105 (2019).
247. N. V. Chernomyrdin et al., "Reflection-mode continuous-wave 0.15λ-resolution terahertz solid immersion microscopy of soft biological tissues," *Appl. Phys. Lett.* **113**, 111102 (2018).
248. N. V. Chernomyrdin et al., "A potential of terahertz solid immersion microscopy for visualizing sub-wavelength-scale tissue spheroids," *Proc. SPIE* **10677**, 106771Y (2018).
249. L. Yue et al., "A millimetre-wave cuboid solid immersion lens with intensity-enhanced amplitude mask apodization," *J. Infrared, Millimeter, Terahertz Waves* **39**, 546–552 (2018).
250. N. V. Chernomyrdin et al., "Solid immersion terahertz imaging with sub-wavelength resolution," *Appl. Phys. Lett.* **110**, 221109 (2017).
251. M. A. Salhi, I. Pupeza, and M. Koch, "Confocal THz laser microscope," *J. Infrared, Millimeter, Terahertz Waves* **31**, 358–366 (2010).
252. I. N. Dolganova et al., "The role of scattering in quasi-ordered structures for terahertz imaging: local order can increase an image quality," *IEEE Trans. Terahertz Sci. Technol.* **8**, 403–409 (2018).
253. N. V. Chernomyrdin et al., "Wide-aperture aspherical lens for high-resolution terahertz imaging," *Rev. Sci. Instrum.* **88**, 014703 (2017).
254. I. Minin and O. Minin, *Diffractive Optics and Nanophotonics*, Springer International Publishing, Cham (2016).
255. I. V. Minin and O. V. Minin, "Experimental verification 3D subwavelength resolution beyond the diffraction limit with zone plate in millimeter wave," *Microwaves Opt. Technol. Lett.* **56**, 2436–2439 (2014).
256. I. V. Minin et al., "Localized photonic jets from flat, three-dimensional dielectric cuboids in the reflection mode," *Opt. Lett.* **40**, 2329 (2015).
257. I. V. Minin, O. V. Minin, and I. S. Nefedov, "Photonic jets from Babinet's cuboid structures in the reflection mode," *Opt. Lett.* **41**, 785 (2016).
258. V. A. Zhelnov et al., "FDTD-modelling of terahertz solid immersion microscopy," *Proc. SPIE* **11164**, 111640H (2019).
259. N. V. Chernomyrdin et al., "Terahertz microscope based on solid immersion effect for imaging of biological tissues," *Opt. Spectrosc.* **126**, 560–567 (2019).
260. V. A. Trofimov and V. V. Trofimov, "New way for concealed object detection using passive THz images without their viewing," *Proc. SPIE* **9651**, 96510A (2015).
261. M. S. Kulya et al., "Computational terahertz imaging with dispersive objects," *J. Mod. Opt.* **64**, 1283–1288 (2017).
262. A. Siemion et al., "Off-axis metallic diffractive lens for terahertz beams," *Opt. Lett.* **36**, 1960–1962 (2011).
263. A. Siemion et al., "Diffractive paper lens for terahertz optics," *Opt. Lett.* **37**, 4320 (2012).
264. A. Siemion et al., "THz beam shaping based on paper diffractive optics," *IEEE Trans. Terahertz Sci. Technol.* **6**, 568–575 (2016).
265. A. I. Hernandez-Serrano et al., "Fabrication of gradient-refractive-index lenses for terahertz applications by three-dimensional printing," *J. Opt. Soc. Am. B* **33**, 928 (2016).
266. K. Ahi, "Lithography, spectroscopy, and super resolution terahertz imaging for quality assurance and authentication," Doctoral Dissertation, University of Connecticut (2017).
267. K. Ahi, "Mathematical modeling of THz point spread function and simulation of THz imaging systems," *IEEE Trans. Terahertz Sci. Technol.* **7**, 747–754 (2017).
268. K. Ahi, "A method and system for enhancing the resolution of terahertz imaging," *Measurement* **138**, 614–619 (2019).
269. K. Ahi, "Method and system for enhancing resolution of terahertz imaging," US Patent Application.
270. A. Kannegulla and L.-J. Cheng, "Subwavelength focusing of terahertz waves in silicon hyperbolic metamaterials," *Opt. Lett.* **41**, 3539 (2016).
271. N. S. Balbekin et al., "Increasing the resolution of the reconstructed image in terahertz pulse time-domain holography," *Sci. Rep.* **9**, 180 (2019).

272. M. Kulya et al., "Hyperspectral data denoising for terahertz pulse time-domain holography," *Opt. Express* **27**, 18456 (2019).
273. M. Kulya et al., "Terahertz pulse time-domain holography with balance detection: complex-domain sparse imaging," *Appl. Opt.* **58**, G61 (2019).
274. F. Qian et al., "A memristor-based compressive sensing architecture," in *Proc. 2016 IEEE/ACM Int. Symp. Nanoscale Architect.*, IEEE (2016).
275. L. Angrisani et al., "Experimental performance assessment of compressive sampling-based THz imaging systems," in *IEEE Int. Instrum. Meas. Technol. Conf.*, IEEE, pp. 1–6 (2017).
276. L. Angrisani et al., "On the measurement uncertainties of THz imaging systems based on compressive sampling," *Measurement* **116**, 83–95 (2018).
277. E. M. Stübling et al., "Application of a robotic THz imaging system for sub-surface analysis of ancient human remains," *Sci. Rep.* **9**, 3390 (2019).
278. E. Stübling et al., "A THz tomography system for arbitrarily shaped samples," *J. Infrared, Millimeter, Terahertz Waves* **38**, 1179–1182 (2017).

Kiarash Ahi received his MSc degree in electrical and information engineering from the Leibniz University of Hannover, Germany, in 2012 and his PhD in electrical and computer engineering (ECE) from the University of Connecticut in 2017. The focus of his MSc degree was smart grid, renewable energy systems, and power electronics. His PhD studies were in the areas of semiconductor technology, optics, machine learning and natural computation, compressive sensing, and terahertz (THz) signal and image processing. Currently, he is a senior researcher and lead product development engineer in the advanced semiconductor and software industry, where he researches areas where artificial intelligence can enhance the accuracy and efficiency of semiconductor device manufacturing toward driving Moore's law. He architects automated systems, empowered by machine learning and image processing, and leads multinational R&D teams. His scientific and research interests include digital image and signal processing, optics and photolithography, MEMS and semiconductor devices, machine learning and artificial intelligence, hardware security, bioengineering, wearable technologies, embedded systems, human–computer interaction, THz technology, and intelligent software development.

Nathan Jessurun is currently a PhD student at the University of Florida in the ECE Department. He received his BS degree in computer engineering from Cedarville University in 2019. Currently, his research is focused on bimodal imaging applications, THz imaging for hardware characterization, and developing novel image processing techniques.

Mohammad-Parsa Hosseini is a senior member at IEEE. He received his PhD in ECE with research in computer science from Rutgers University, New Jersey, in 2018. He had previously received his BSc degree in electrical and electronic engineering in 2006, a graduate study in MSc of biomedical engineering in 2008, and a second MSc program in electrical and communication engineering in 2010. He is collaborating with the Medical Image Analysis Lab at Henry Ford Health System and with the Clinical Neurosciences Department, Spectrum Health, Michigan. He has worked as a senior data scientist and machine learning researcher in Silicon Valley, California, since 2017. He has been a university adjunct lecturer and a faculty member since 2009 and currently is with Santa Clara University. His current interests are in the areas of machine learning, deep learning, signal and image processing. He has served on the scientific committees and review boards of several national and international conferences and journals.

Navid Asadizanjani received his PhD in mechanical engineering from the University of Connecticut in 2014. He is an assistant professor in the ECE Department at the University of Florida, Gainesville. His primary research interests include physical attacks and inspection of electronics. He has received several best paper awards from the International Symposium on Hardware Oriented Security and Trust and International Symposium on Flexible Automation. He has also received the D.E. Crow Innovation award from the University of Connecticut. He is the program chair of the PAINE conference and serves on the technical program committee of the International Symposium for Testing and Failure Analysis and IEEE Computing and Communication Workshop and Conference.